

# Accepted Manuscript

Geochemical constraints on the role of tuffisite veins in degassing at the 2008–09 Chaitén and 2011–12 Cordon Caulle rhyolite eruptions

R. Paisley, K. Berlo, B. Ghaleb, H. Tuffen



PII: S0377-0273(18)30496-7

DOI: <https://doi.org/10.1016/j.jvolgeores.2019.05.013>

Reference: VOLGEO 6614

To appear in: *Journal of Volcanology and Geothermal Research*

Received date: 31 October 2018

Revised date: 25 April 2019

Accepted date: 13 May 2019

Please cite this article as: R. Paisley, K. Berlo, B. Ghaleb, et al., Geochemical constraints on the role of tuffisite veins in degassing at the 2008–09 Chaitén and 2011–12 Cordon Caulle rhyolite eruptions, *Journal of Volcanology and Geothermal Research*, <https://doi.org/10.1016/j.jvolgeores.2019.05.013>

This is a PDF file of an unedited manuscript that has been accepted for publication. As a service to our customers we are providing this early version of the manuscript. The manuscript will undergo copyediting, typesetting, and review of the resulting proof before it is published in its final form. Please note that during the production process errors may be discovered which could affect the content, and all legal disclaimers that apply to the journal pertain.

**Geochemical constraints on the role of tuffisite veins in degassing at the 2008-09  
Chaitén and 2011-12 Cordón Caulle rhyolite eruptions**

R. Paisley\*, <sup>1</sup>, K. Berlo<sup>1, 2</sup>, B. Ghaleb<sup>2</sup>, H. Tuffen<sup>3</sup>

\*correspondence email: rebecca.paisley@mail.mcgill.ca

<sup>1</sup>Department of Earth & Planetary Sciences, McGill University, 3450 Rue University,  
Montreal, Quebec, Canada, H3A 0E8

<sup>2</sup>Geotop, Université du Québec à Montréal, Montréal, Canada

<sup>3</sup>Lancaster Environment Centre, Lancaster University, Lancaster, UK

**Highlights:**

- Multi-stage degassing signatures preserved in Chaitén's tuffisite veins
- The erupted products at both volcanoes preserve minimal <sup>210</sup>Pb-<sup>226</sup>Ra disequilibria
- Geochemical preservation of gas fluxing through tuffisite veins at Cordón Caulle
- Evidence of preferential transport of glass over crystals in tuffisite veins

## Abstract

Hybrid activity during the rhyolitic eruptions of Chaitén (2008-09) and Cordon Caulle (2011-2012) in Chile has offered unprecedented insights into the enigmatic and complex degassing processes occurring during eruptions of silicic magma. Highly permeable, transient fracture networks within the conduit can act as outgassing channels. Their interaction with deeper volatile-rich melt can account for both punctuated explosive activity and large-scale degassing of the system, leading towards predominantly effusive behaviour. In this study we characterise trace element concentrations and  $^{210}\text{Pb}$ - $^{226}\text{Ra}$  systematics within pyroclastic material from the recent eruptions at Chaitén and Cordon Caulle volcanoes. Results reveal how gas fluxing from deep, volatile-rich reservoirs to the surface, within magmatic conduits, can be recorded by trace elements and  $^{210}\text{Pb}$ - $^{226}\text{Ra}$  disequilibria in tuffisite veins.

Tuffisite veins (particle-filled fracture networks) are present in volcanic bombs from both eruptions. Trace element heterogeneity associated with tuffisites preserves evidence for degassing. At Chaitén, enrichments (e.g. Cu) and depletions (e.g. Mo, Li and Bi) are identified in vein material and clasts transported within veins, and record multiple degassing events. At Cordon Caulle, enrichments of volatiles in an early vein (e.g. Tl and Bi) and depletions in a later vein (e.g. Cd, In, Pb and Tl) reflect interactions between glassy clasts and the carrier gas phase that transported them. In contrast,  $^{210}\text{Pb}$  and  $^{226}\text{Ra}$ , which can be fractionated during degassing, are mostly in secular equilibrium. Modelling suggests that the disparity between the signals preserved in these two types of chemical signatures reflects the brevity of degassing events and the relative volumes of tuffisite veins and the bodies of degassing magma that they source gas from. The lack of preserved  $^{210}\text{Pb}$  enrichments in

tuffisite veins at both volcanoes places an upper limit on the mass of deeper, bubble-rich magma outgassed via tuffisites during their lifetime.

This study shows that both the presence, and absence, of sample-scale geochemical heterogeneity can be used to place constraints on syn-eruptive physical processes and underlines the value of analysing a wide suite of trace element species.

**Key Words:**

- Degassing
- Tuffisite Veins
- $^{210}\text{Pb}$ - $^{226}\text{Ra}$  Disequilibria
- Magma Fracturing
- Rhyolitic Eruptions

**1. Introduction**

Volatile behaviour during magma ascent governs eruption style at the surface and is recorded in the erupted deposits (Gonnermann and Manga, 2007, Edmonds, 2008). Silicic eruptions commonly shift from explosive to effusive activity with time, despite no change in the initial magma volatile content (Eichelberger et al., 1986, Jaupart and Allègre, 1991). The observation of hybrid activity – simultaneous Vulcanian explosions and lava effusion – during recent rhyolitic eruptions at Chaitén (2008-09) and Cerdón Caulle (2011-2012) calls

for an investigation into the processes that facilitate the long-term transition towards predominantly effusive behaviour (Schipper et al., 2013, Pallister et al., 2013a). Fracture networks have been hypothesised as permeable degassing pathways within the magma-filled conduit that are transient in time and space. They facilitate the extensive degassing of a system during an eruption and a shift to effusive behaviour, while also accounting for punctuated pressurisation and resulting Vulcanian explosions (Stasiuk et al., 1996, Schipper et al., 2013, Kendrick et al., 2016). These transient fractures, sometimes preserved as particle-filled tuffisite veins, can be up to three orders of magnitude more permeable than their hosts when open, before sintering and compaction of particles within veins dramatically reduces permeability (Kolzenburg et al., 2012, Heap et al., 2015, Farquharson et al., 2016).

Whilst fractures can act as gas pathways spanning hundreds of metres within the conduit (Castro et al., 2012, Berlo et al., 2013, Castro et al., 2014, Saubin et al., 2016), the degree of interaction between veins and gas-rich sources at depth is poorly constrained. There is a need to quantify how much melt a fracture can degas during its lifespan in order to assess its potential impact on eruption mechanisms. Here we present a trace element and  $^{210}\text{Pb}$ - $^{226}\text{Ra}$  isotope study of volcanic bombs from both Chaitén and Cordon Caulle in Chile, sourced from the upper conduit plugs from these two volcanoes, as inferred by low residual water concentrations in volcanic bombs from these eruptions (Schipper et al., 2013, Castro et al., 2014). We focus on tuffisite veins to assess geochemical evidence of gas flow through these highly permeable features. The preservation of syn-eruptive degassing signatures allows for a quantitative constraint on the interaction between transient fracture pathways and deeper volatile-rich, magma sources. We find that whilst trace element signatures at both volcanoes can be related to degassing and other physical processes, degassing-induced isotopic disequilibrium in veins is lacking. The disparity between isotopic and trace element

signatures at Chaitén and Cordon Caulle relate to the duration of gas fluxing and the contrasting nature of the upper conduit conditions during the two eruptions, including the fracturing depth and gas compositions.

## 1.1 Tuffisite Veins

Tuffisite veins are fractures filled and propped open by variably sintered, fine-grained material (with particle sizes spanning microns to centimetres). Their lengths can span from centimetres to hundreds of metres within conduits, country rock and bombs ejected during Vulcanian explosions (e.g. Stasiuk et al. (1996), Tuffen and Dingwell (2005), Castro et al. (2012), Castro et al. (2014)). Veins and fractures result from brittle fracture of magma and country rocks, triggered either by high shear strain rates (Tuffen et al., 2003) or hydrofracturing (Heiken et al., 1988), thus opening potential gas pathways (Gonnermann and Manga, 2003). The lifespan of the veins ends with the sintering and compaction of vein-filling clasts (Tuffen et al., 2003, Kendrick et al., 2016, Saubin et al., 2016). A reduction in the permeability of magma within the upper conduit, the result of processes including viscous densification and porosity loss, can lead to repeated cycles of volatile accumulation, fracturing, gas escape via explosions, and healing of magma on ascent (Okumura and Sasaki, 2014, Heap et al., 2015). This is recorded texturally as anastomosing, cross-cutting veins that preserve evidence of transient fluidised flow as well as subsequent sintering, compaction and ultimately complete destruction of primary porosity and permeability within the vesicle-poor upper conduit (Stasiuk et al., 1996, Tuffen et al., 2003, Tuffen and Dingwell, 2005). Fracturing can briefly create a highly permeable pathway and deplete major volatiles in the neighbouring dense melt, but only localised depletions develop, within hundreds of microns

of fracture surfaces. In this case, repeated, mm-scale brecciation would be required for effective degassing (Okumura et al., 2010, Castro et al., 2012). Thus, for melt fracturing to be an enabler of efficient degassing it must provide a pathway for gases to escape from more permeable, vesicular magmas at depth through the vesicle-poor ‘plug’ in the upper conduit. Element enrichment in tuffisite veins and detailed textural records of intra-vein clasts show evidence for this interaction with deeper magma and gases, for example using H<sub>2</sub>O differences between tuffisite clasts and host material as a proxy for depth at Chaitén, vein connectivity is shown to occur ~150 metres (Berlo et al., 2013, Castro et al., 2014, Saubin et al., 2016). However, questions remain over what mass of magma can be efficiently degassed by a tuffisite during its lifespan, which we address with a combination of trace element and <sup>210</sup>Pb-<sup>226</sup>Ra isotope analyses of veins.

## 1.2 Volatiles, trace species and Ra-Rn-Pb systematics during degassing

A volcanic vapour phase is dominated by major volatile species (e.g. H<sub>2</sub>O, CO<sub>2</sub>, S, Cl and F) that act as complexing agents for semi-volatile metals (e.g. Cu, Tl, Sn), and carrier gases for low concentration volatiles (e.g. Rn, Po) that can be enriched in gas plumes and at fumaroles (Lambert et al., 1985, Hinkley et al., 1994, Williams-Jones et al., 2002). As metal-bearing gases stream through fractures they interact with melt-rich clasts being carried by the gas, as well as the surrounding host melt. Fluxing will end when gas supply ceases or clasts sinter and compact, sealing the vein. Conditions (e.g. pressure, temperature, oxygen fugacity) can change within fractures during gas fluxing, affecting the vapour-melt partition coefficients of metals and the stability of their complexing agents (Williams-Jones and Heinrich, 2005), and induce chemical heterogeneity in the vein material and neighbouring fracture host melt.

Metals can be scavenged from clasts resulting in depletions, e.g. Berlo et al. (2013), or deposited onto clast surfaces via adsorption forming metal-bearing mineral phases as seen in fumaroles resulting in enrichments, e.g. Williams-Jones et al. (2002) and Berlo et al. (2013). If conditions allow volatile elements in the gas phase can re-equilibrate with the surrounding melt and be reabsorbed into the melt structures also leading to metal enrichments, e.g. Plail et al. (2014).

The Uranium ( $^{238}\text{U}$ ) decay-series contains many short-lived isotopes with varied geochemical properties and half-lives ( $t_{1/2}$ ). Fractionating processes such as crystallisation, partial melting or changing oxygen fugacity ( $f\text{O}_2$ ), can cause disequilibrium between different isotopes within the series (e.g. Bourdon et al, 2003; Berlo and Turner, 2010 and references therein). Degassing can induce disequilibrium between  $^{226}\text{Ra}$ ,  $^{222}\text{Rn}$  and  $^{210}\text{Pb}$ .  $^{210}\text{Pb}$ - $^{226}\text{Ra}$  disequilibria have been used to study the timing and redistribution of Rn-rich gases from deeper to shallower magmas in recent andesitic and dacitic eruptions including Mt St Helens (USA), Rabaul (Papa New Guinea) and Mt Pinatubo (Philippines) (Berlo et al., 2006, Cunningham et al., 2009, Kayzar et al., 2009). During degassing  $^{222}\text{Rn}$  ( $t_{1/2} = \sim 3.8$  days), the volatile daughter isotope of  $^{226}\text{Ra}$  ( $t_{1/2} = \sim 1600$  years), prefers the exsolved gas phase. With time  $^{222}\text{Rn}$  decays through several short-lived intermediate daughters to  $^{210}\text{Pb}$  ( $t_{1/2} = 22.6$  years), which is less volatile and resorbed back into the melt (Lambert et al., 1985). Persistent gas-melt segregation can result in the redistribution of the nuclides between melt that has lost gas and melt that has undergone gas fluxing. It is recorded in the erupted products as  $^{210}\text{Pb}$  ‘deficits’, where  $(^{210}\text{Pb}/^{226}\text{Ra}) < 1$ , and  $^{210}\text{Pb}$  ‘excesses’, where  $(^{210}\text{Pb}/^{226}\text{Ra}) > 1$ . Here we characterise  $^{210}\text{Pb}$ - $^{226}\text{Ra}$  disequilibria to quantify interactions between tuffisites and deeper magma and their exsolved gases.



### 1.3 Two Case Studies: Chilean Rhyolites

Chaitén and Cordon Caulle volcanoes both within the Chilean Southern Volcanic Zone (SVZ), produced the world's most recent rhyolitic eruptions in 2008 and 2011 respectively. The two eruptions have many similarities in both their eruption dynamics and eruptive products. Chaitén erupted unexpectedly on May 1<sup>st</sup> 2008 with two weeks of explosive activity ( $\sim 0.3 \text{ km}^3$  dense rock equivalent, DRE), with a  $< 21 \text{ km}$  eruption column before transitioning into 20 days of hybrid activity (Pallister et al., 2013a, Major and Lara, 2013). Dome extrusion ( $\sim 0.8 \text{ km}^3$ ) continued until late 2009 (Major and Lara, 2013). The 2011-2012 eruption of Cordon Caulle commenced on June 4th with a persistent  $< 15 \text{ km}$  high Plinian eruption column for 27 hours, that transitioned into sub-Plinian behaviour, with lava effusion starting  $\sim 11$  days later and simultaneous emplacement of a shallow (20-200 m deep) laccolith (Silva Parejas, 2012, Castro et al., 2016). The eruption continued into a prolonged phase of explosive activity accompanied by lava effusion that terminated in March 2012 with  $\sim 1.4 \text{ km}^3$  DRE of magma being erupted in total (Tuffen et al., 2013, Pistolesi et al., 2015), together with  $\sim 0.8 \text{ km}^3$  of magma intruded within the laccolith. Chaitén magma was sourced from a depth of  $\sim 5 \text{ km}$  ( $\sim 50$ -200 MPa),  $\sim 780$ -825 °C, (Castro and Dingwell, 2009) while depth estimates for Cordon Caulle range from 2.5 km to 7 km (895-920 °C,  $f\text{O}_2 \sim \text{QFM}$ ); and both are volatile-saturated at depth (Castro et al., 2013a, Jay et al., 2014). Erupted products for both eruptions are sparsely phyrlic ( $< 5 \text{ vol. \%}$ ), particularly the earlier explosively erupted material. Chaitén has a phenocryst assemblage of plagioclase, orthopyroxene and Fe-Ti oxides with rare biotite. The Cordon Caulle assemblage is similar, with plagioclase, orthopyroxene and Fe-Ti oxides, plus additional clinopyroxene, and accessory apatite and

pyrrhotite (Castro and Dingwell, 2009, Castro et al., 2013a). Recorded precursory activity at Chaitén was on the order of hours compared to the months of heightened seismic activity and years of pre-eruptive inflation phases at Cordon Caulle, although there is a recording bias as no seismometers were placed close to Chaitén prior to the 2008 eruption. The effusive components to the eruptions differ, with a dome forming at Chaitén whilst a lava flow formed at Cordon Caulle. The groundmass glass water concentrations of the final products from each eruption are markedly different. Chaitén samples vary from ~0.1 to 1.6 wt. % H<sub>2</sub>O and have been used to trace degassing in the upper ~1 km of the conduit, whereas Cordon Caulle samples are ubiquitously degassed to near-atmospheric pressures (<0.35 wt. % H<sub>2</sub>O) (Schipper et al., 2013, Castro et al., 2014), and are thought to reflect an origin in the upper 200 metres of the conduit.

## 2. Methods

Tuffisite veins and other sub-samples were cut and isolated from their host hand specimens with a micro-rotary tool and powdered with a pestle and mortar. Aliquots of powders, weighing 0.1-0.9 g, underwent closed vessel digestion in a concentrated HF-HNO<sub>3</sub>-HCl-H<sub>3</sub>BO<sub>3</sub> mixture. After digestion, solutions were centrifuged, and any insoluble materials were re-attacked until sample solutions appeared clear. Separate powder aliquots were digested for Po isotope, Ra isotope and trace element determinations. <sup>210</sup>Pb ( $t_{1/2}$  = 22.6 years) activities were determined via alpha-spectrometry of its granddaughter isotope <sup>210</sup>Po ( $t_{1/2}$  = 138.4 days), as secular equilibrium between the two is re-established ~2 years after eruption. Samples were analysed a minimum of 4 years after eruption and thus it is valid to use <sup>210</sup>Po as a proxy for <sup>210</sup>Pb (Bourdon et al., 2003). To determine <sup>210</sup>Po, a weighed drop of <sup>209</sup>Po spike was dried

down in Teflon and sample powders then added, digested, and taken up in 0.5N HCl. Po was autoplated on Ag disks and counted on an alpha spectrometer (EGG-ORTEC at GEOTOP, Université de Quebec à Montreal) for a minimum of 7 days. Some samples underwent an additional chromatographic column purification step, summarised in Reagan et al. (2005), prior to plating. We found no difference in the  $^{210}\text{Pb}$  activity between the two methods, however the latter chromatography method produced spectra with a reduced low-energy tail length and less noise, defining a clearer peak.  $^{226}\text{Ra}$  activities were determined with a VG sector 54 Thermal Ionisation Mass Spectrometer (TIMS) using a  $^{228}\text{Ra}$  spike calibrated against 15 aliquots of BCR-2 powder, that underwent the digestion procedure described above, with an assumed ( $^{226}\text{Ra}$ ) of 1.26 dpm/g. The Ra chemistry followed the procedure from Ghaleb et al. (2004). BCR-2 was regularly analysed, as an unknown, for both  $^{210}\text{Pb}$  and  $^{226}\text{Ra}$  and found to be within error of calculated  $^{238}\text{U}$  activities and published values, e.g. Cunningham et al. (2009), on all occasions. Procedural blanks, carried out regularly for both isotope systems, showed  $^{210}\text{Po}$  counts to be below background and negligible  $^{226}\text{Ra}$ . Isotope analyses were conducted between 2014 and 2017, ( $^{210}\text{Pb}$ )<sub>o</sub> and errors are back-calculated to correct for time between eruption and analysis using the decay equation (Berlo and Turner, 2010). Bracketed isotopes, e.g. ( $^{210}\text{Pb}$ ), denote isotope activities or isotope activity ratios. Trace element concentrations were measured using a Thermo Scientific iCAP Q ICP-MS at McGill University on 2 %  $\text{HNO}_3$  dilutions. Rock standards BCR-2 and UTR-2 were analysed to assess for accuracy and fall within error of published values (Appendix A). Samples were digested in three sessions in May 2016, November 2016 and November 2017. Calibration standards were prepared from multi-element, ICP-MS grade, standard solutions with trace metal grade acids and nano pure water. Up to 9 standards were prepared and diluted to cover the range of expected concentrations. New calibration standards were prepared for each session and a minimum of two analyses per standard, per session were collected to correct for

drift. Calibration curves for each element, in each session, were calculated via a robust, linear regression fit through a minimum of 3 calibration standards. Both sample and analytical duplicates were run in each session and data collected in November 2016 and 2017 were median-normalised to the May 2016 dataset. Relative standard deviations (% RSD) were calculated via duplicates in each session for each sample, see Appendix A for calculated errors.

### **3. Results**

#### **3.1 Sample Petrology**

Samples from both volcanoes were selected based on textural features that are indicative of upper conduit fragmentation and localised gas-loss during the transitional phases of both eruptions. Bombs are dense, partially foamed or fully pumiceous and, in addition, can be vein-bearing or brecciated with varying degrees of welding. All sub-samples are described in Figure 1. Two metre-scale bombs from the 2008 Chaitén eruption were collected from inside the crater, from pyroclastic density current deposits, and represent dense, tuffisite-hosting (Bomb A) and breadcrust (Bomb B) bombs, two textural types typical of bombs from the hybrid phase of activity that occurred between the 11<sup>th</sup> and 31<sup>st</sup> of May, 2008 (Castro et al., 2012, Saubin et al., 2016). Bomb A (also described as BTB) is a 30 x 40 x 50 cm dense obsidian bomb found ~800 m from the vent and is extensively described in Saubin et al. (2016). The central tuffisite vein is approximately 3 cm-wide and filled with mm to cm-sized dense obsidian, pale vesicular and banded or crystalline clasts, all set in a fine-grained matrix.

Smaller  $\mu\text{m}$  to  $\text{mm}$ -sized subsidiary veins propagate from, and are found sub-parallel to, this central vein. Bomb B is  $\sim 1$  m-across, with a dense (2-8 cm) rind that grades into an exposed pumiceous interior. Grey-black (mm-wide) glassy bands delineate separate clasts of white pumice in the bomb interior, with band density increasing towards the bomb edge. Clasts have micro-porosity away from these dense bands and secondary breadcrusting is observed on the exposed faces of some clasts. Six samples (five bombs and one lava sample) from the 2011-2012 eruption of Cordon Caulle represent the different bomb types observed, and the explosive and effusive products of the hybrid activity that commenced after the initial Plinian phase in June 2011 (Castro et al., 2013b). At Cordon Caulle, Bombs 1 and 2 were collected from a ridge  $\sim 3.5$  km NW of the vent and three further samples (Bombs 3-5) were collected from the vent area within the tephra cone. Bombs found far from the vent (Bombs 1-2) were ejected in explosions during a low intensity explosive phase (7<sup>th</sup> June onwards) and beginning phase of hybrid activity (Schipper et al., 2013, Pistolesi et al., 2015). (Schipper et al., 2013, Pistolesi et al., 2015). Bombs were observed being ejected  $< 1$  km from the vent in January 2012 (Schipper et al., 2013) and thus we assume Bombs 3-5 represent the explosive component of the later, waning hybrid activity as they were collected from the tephra cone that built up during the eruption, within 300 m of the vent opening. Veins in Bombs 2 and 3 are predominantly filled by well-sorted, fine ash (Figure 1). The tuffisite vein in Bomb 2 is  $\sim 1$ -3 cm wide and is laterally continuous throughout the rind of the bomb. Reservoir zones, irregular voids filled by micron-sized ash material that offshoot from central veins as described by Tuffen and Dingwell (2005), can be  $< 7$  cm wide. Tuffisite material in Bomb 3 is hosted in concave voids (approximately 5cm-wide and 3 cm-deep) that are part of a series of large coalesced vesicles in this highly sheared sample. The infiltration and clogging of the small vesicles in the neighbouring host by the tuffisite appear to have sealed this large coalesced vesicle train, isolated it from others, and concentrated gas transport along this one

path. Bomb 4 is a ~4cm-wide multi-component vein, with coarse-grained beds composed of dense obsidian clasts and glassy, oxidised (pink-coloured), micron-sized ash; and fine-grained beds of heavily sintered glassy ash, which could represent tapping of a more complex heterogeneous conduit (Saubin et al., 2016). The relative timing of the degassing events that resulted in Bombs 3 and 4 are hard to definitively distinguish. Bomb 3 has tuffisite textures commonly seen in bombs ejected during the early phase of the eruption (e.g. Bomb 2) whilst Bomb 4 is more welded and heterogeneous. Thus, we suggest that Bomb 4 likely was erupted later than Bomb 3, and underwent more extensive compaction, but both were later than Bomb 2. The Cordon Caulle obsidian flow (Flow 1) was sampled from a breakout on the NW front of the northern branch that was impeded by a ridge within 60 days of the eruption commencing (Magnall et al., 2017, Magnall et al., 2018).

### 3.2 $^{210}\text{Pb}$ - $^{226}\text{Ra}$ Isotopes

$^{210}\text{Pb}$  and  $^{226}\text{Ra}$  data for Chaitén and Cordon Caulle are presented in Figure 2 and Table 1. Sub-samples of volcanic bombs from Chaitén have activity ratios within error of secular equilibrium, with the exception of Bomb B Exterior ( $(^{210}\text{Pb}/^{226}\text{Ra})_o = 0.83 \pm 0.12$ ), whose depletion results from higher  $^{226}\text{Ra}$  and lower  $^{210}\text{Pb}$  activities. At Cordon Caulle, earlier activity samples (Flow 1, Bombs 1-2), Bomb 3 and the host component of Bomb 4 have  $(^{210}\text{Pb}/^{226}\text{Ra})_o$  activities within error of 1. Bomb 4 (vein) is depleted in  $^{210}\text{Pb}$  relative to  $^{226}\text{Ra}$ ,  $(^{210}\text{Pb}/^{226}\text{Ra})_o = 0.90 \pm 0.02$ . Bomb 5 is slightly enriched in  $^{210}\text{Pb}$  relative to  $^{226}\text{Ra}$ ,  $(^{210}\text{Pb}/^{226}\text{Ra})_o = 1.19 \pm 0.17$ .

### 3.3 Trace Elements

The measured trace element abundances of each sample are given in Appendix A, and highlights are discussed below. For ease of comparison elements are grouped into four categories based on their properties and similar behaviours (White, 2013). Group 1 elements (Mg, P, Sc, V, Mn, Co and Sr) are highly compatible in the crystallising assemblages and Group 2 elements (Be, Ga, Ba, La, Ce, Pr, Nd, Sm, Eu, Gd, Tb, Dy, Ho, Er, Tm, Yb, Lu, Y and Th) are the rare earth elements (REEs) and other moderately incompatible elements. Group 3 elements (Zr, Nb, Hf, Ta and U) are the high field strength elements (HFSEs) and U. Group 4 elements (Li, Rb, Cs, Mo, Ag, Cd, In, Sn, Sb, W, Tl, Pb, Bi, Cu, Zn) are a collection of elements known to partition into magmatic and hydrothermal fluids and vapours by forming chloride, sulphide, fluoride and hydroxy complexes (e.g. Webster (1990), Churakov et al. (2000), Wahrenberger (2002), Zajacz et al. (2008), Pokrovski et al. (2013) and references therein). Elemental concentrations of tuffisite veins from Chaitén (Figure 3) and Cordon Caulle (Figure 4) are compared to their respective hosts.

#### 3.3.1 Chaitén

The higher  $^{210}\text{Pb}$  and  $^{226}\text{Ra}$  activities and concentrations of incompatible elements (e.g. Th, U, Appendix A) reflect the more evolved magma at Chaitén, ~75 wt. %  $\text{SiO}_2$  (Pallister et al., 2013a) compared to ~70 wt. %  $\text{SiO}_2$  (Castro et al., 2013a) at Cordon Caulle. Trace element concentrations across both sub-samples of Bomb B and Bomb A (Host) are within error of each other and are similar to samples analysed by Pallister et al. (2013b), supporting the

theory that melt for this eruption is near homogeneous in major and trace elements and similar to historical Holocene eruptions (Lowenstern et al., 2012). Group 1 and Group 2 elements plus select elements from Group 4 (Zn, Sn, Tl and Pb), in particular, show little variation across both bombs.

However, on a cm-mm scale elemental variation does occur. In the vein material of Bomb A and Banded Clast, a non-juvenile clast type that accounts for ~42% of the vein (Saubin et al., 2016), elemental variation is best studied by examining the compositions vein-host ratio, e.g.  $Li_{\text{vein}}/Li_{\text{Host}}$ , allowing for an easy comparison of composition (Figure 3). When compared to the host composition, Group 3 elements are depleted in both the vein material and Banded Clast, along with many Group 4 elements (Figure 3). The Banded Clast has stronger depletions of Bi, Li, Mo, W, Ag, and Cd (ratios averaging ~0.58 when compared to the host) than the vein material (average ratios ~0.88). Cu is depleted within the Banded Clast but shows enrichment in the vein matrix ((2-column) Figure 3: Select elemental concentrations of Vein Matrix, Vein Matrix & Clasts (bulk tuffisite) and Banded Clast normalised to Bomb A Host composition (Chaitén Volcano). Depletions in HFSEs and volatile elements (e.g. Mo, Li, Bi) are evident in both clast and vein samples, as is Cu enrichment in the vein. Errors are 2 standard deviation.

3). The Banded Clast is enriched in Ni relative to all other samples (not shown in Figure 3).

### 3.3.2 Cordón Caulle



At Cordón Caulle, Group 2 and 3 elements, and select Group 4 elements (Li, Mo, Ag, Sb and Zn), show little variation across the sample suite (see Appendix A). Key observations noted in elemental variation of samples are: (1) Bomb 2 (Interior) is elevated in Cu and Sn over the rest of the samples; (2) Bomb 3 is enriched in Bi and depleted in P and In with respect to the average Cordón Caulle composition; and (3) the host component of Bomb 3 is further enriched in Tl.

When vein material from Bomb 2, Bomb 3 and Bomb 4 are compared to their respective hosts a similar ratio signature pattern between veins is observed (Figure 4). Veins are depleted in Group 1 elements. Group 2 and 3 elements are similar in the veins to their respective hosts. Group 4 elements show variability within the veins. Bi is enriched in veins in Bombs 2-3. The vein in Bomb 2 is enriched in Tl. The vein from Bomb 3 has an apparent depletion in Tl relative to the host, but the depletion is exaggerated due to the host's higher than average Tl concentration ( $0.8 \pm 0.3$  ppm vs an average of  $0.43 \pm 0.07$  ppm). The vein in Bomb 4 is depleted in Cd, In, Tl and Pb, and enriched in Cu and Rb.

#### 4. Discussion

Neither Chaitén nor Cordón Caulle have significant  $^{210}\text{Pb}$ - $^{226}\text{Ra}$  disequilibria, however trace element variation is preserved and can be linked to several processes that occur before and during eruption, and at the conduit- and fracture-scales. The discussion is divided into sections that address degassing signatures, other physical processes, and how heterogeneity relates to conditions in the upper conduit. Section 4.1 discusses degassing-induced

heterogeneity in isotopes and trace elements and the implications for the disparity between them. Section 4.2 outlines how the lack of isotope disequilibria within fractures can be used to constrain the mass of melt that outgas via a fracture during their open lifespans, we use Chaitén as an example before discussing its applicability to other systems. We discuss trace element variations that can be attributed to other processes in Section 4.3 and the anomalous  $^{210}\text{Pb}$ - $^{226}\text{Ra}$  disequilibria in Section 4.4. Finally, the last section links the preservation of chemical heterogeneity to the physical conditions of the upper conduit and summarises the potential causes for differences in chemical signatures between these two volcanic eruptions.

#### **4.1 Degassing-induced chemical heterogeneity**

##### **4.1.1 Isotopic Evidence for Degassing**

Disequilibria in  $^{210}\text{Pb}$ - $^{226}\text{Ra}$  isotopes can be preserved at a conduit scale and induced by both pre-eruptive and syn-eruptive degassing (Berlo and Turner, 2010). Therefore it is important to first assess for any heterogeneity between samples before assessing disequilibria within samples related to individual fracturing events.

##### **Pre-Eruptive Degassing**

The majority of samples at Chaitén and Cerdón Caulle are in secular equilibrium, and this lack of large-scale  $^{210}\text{Pb}$ - $^{226}\text{Ra}$  disequilibria indicates no extensive, pre-eruptive degassing

was recorded in the magmas at either volcano. At Chaitén the last recognized eruption was a few hundred years before present, and there was no extensive documented precursory activity prior to the 2008 eruption to indicate the accumulation of shallow magma, thus it is unlikely a large volume of degassing magma was present below this system (Major and Lara, 2013, Amigo et al., 2013). Similarly, at Cordon Caulle, whilst the two previous eruptions occurred in the last 100 years (1922 and 1960), any moderate  $^{210}\text{Pb}$  excesses or deficits produced during these eruptions would be nearing re-equilibration today, given the 58-96 years between the eruptions and 2018, and  $^{210}\text{Pb}$  being within ~94 % of  $^{226}\text{Ra}$  after 4 half-lives (~88 years).

### **Syn-Eruptive Degassing**

Volatile data, including preserved  $\text{H}_2\text{O}$  concentrations (Section 1.3) and trace element variations (Section 4.1.2), from both eruptions suggest that syn-eruptive degassing did occur extensively during these eruptions. However, the main phases of the eruptions were ~12 months in duration, too brief for significant isotopic deficits to form (Gauthier and Condomines, 1999).  $^{210}\text{Pb}$  excesses could be formed within this time (Condomines et al., 2010) but no disequilibria were preserved at either volcano. This suggests there was not enough gas fluxing, Rn transfer, or Rn accumulation within the timeframe of the eruptions to induce significant disequilibria in the Rn system. Similarly, no isotope excesses were recorded in tuffisite veins (within samples), which are channels of volcanic material known to have undergone a large amount of gas fluxing. This lack of disequilibria provides constraints on the degassing through veins and is discussed in Section 4.2.

#### 4.1.2 Trace Element Evidence for Degassing

Heterogeneity preserved in Group 4 elements within sub-samples (e.g. tuffisite veins) from both volcanoes are related to degassing processes. The behaviour of these elements during degassing depend on their melt-vapour partition coefficients (how favourably they will partition into an available vapour) which in turn depends on the ligand availability in the vapour phase (elements they will form complexes with), which vary with pressure and temperature within the conduit (Zajacz et al., 2008, MacKenzie and Canil, 2008, Pokrovski et al., 2013). Their behaviour further depends on their diffusivities in silicic melts (how quickly they will diffuse towards melt-vapour interfaces), which is a function of the H<sub>2</sub>O concentration in the melt, pressure and temperature (Zajacz et al., 2008, MacKenzie and Canil, 2008, Pokrovski et al., 2013). The evolution of these factors during both eruptions is largely unknown and prevents robust and quantitative modelling of trace element partitioning and behaviour. Texturally, tuffisite veins preserve the last major fracturing and degassing event a parcel of melt underwent prior to fragmentation and bomb ejection. Chemical heterogeneity within tuffisite veins largely relate to that final syn-eruptive event. However, it is possible for older degassing events to be preserved within host material and entrained lithics, and so careful sub-sample analyses of differing bomb components allows for the distinction between different events.

**Chaitén**

The biggest compositional variations in the Chaitén samples are within the vein matrix samples and Banded Clast found in the vein of Bomb A (Figure 3). Banded Clasts have previously been interpreted as non-juvenile material from a previous eruption that had undergone shearing events and cristobalite precipitation (Saubin et al., 2016). The clast is depleted in many Group 4 elements, known to be volatile under magmatic conditions (e.g. Mo, Li, Bi, Ag, Cd and Cu), which suggests outgassing occurred simultaneously with these shearing events resulting in the extensive depletion of volatiles in the melt bands within the clast. However, the clast shows no evidence of degassing preserved in its  $^{210}\text{Pb}$  isotope signature. We propose that these clasts are part of the old dome, from a previous eruption that preceded the 2008 eruption by more than 120 years, so any initial disequilibria have been lost. In the less likely scenario it is a juvenile clast, the degassing events recorded as trace element depletions were insufficiently lengthy to be recorded in the  $^{210}\text{Pb}$  isotope signature. Depletions in the Group 3 elements (HFSEs and U) are discussed in Section 4.3.

Cu is enriched in the vein matrix but depleted in the Banded Clast, whilst Bi, Li and Mo are depleted in the vein matrix. Cu, Mo and Sb are among the elements known to be enriched in vein matrices at Chaitén, whilst Li is depleted in the vein matrix but enriched in the pumice clasts within veins (along with Cu and Sb) (Berlo et al., 2013). Bi was not analysed by Berlo et al. (2013). Our bulk vein results appear, at first, contradictory to the in-situ study conducted by Berlo et al. (2013). However, the Mo, Li and Bi depletions in this vein are likely the result of the mixing signature from the Banded Clast overprinting any vein enrichment, as discussed in Section 4.3. Combined, Berlo et al. (2013) and our study show that Cu, Mo, Li, Sb and Bi are mobile and are evidence of gas streaming through tuffisite veins. Gas streaming is the process whereby magmatic gases are channelled through permeable pathways in magma, e.g. fractures that can be preserved as tuffisite veins, which

are transient throughout the conduit during eruption. The ligands present in the gases aid in transporting metals from depth towards the surface, as discussed in Section 1.2, and elements such as Cu, Mo, Sb and Bi are found to more favourably partition into fluids with a low chlorinity, often forming hydroxy complexes (Zajacz et al., 2008, Berlo et al., 2013). Chemical heterogeneity is caused by the interaction of the gases and the transported glass shards and preserves the gas streaming event. The ‘purer’ Vein Matrix sub-sample shows the highest level of Cu enrichment. This could be due to more efficient Cu adsorption onto the finer particles that provide a high surface area for adsorption, or absorption of metals by the sintering melt. The origin of the Cu enrichment remains unclear.

### **Cordón Caulle**

Group 4 elements display a wide range of signatures in the Cordón Caulle veins. Bi and Tl are commonly amongst the most enriched trace elements found in gases, favourably partitioning into available vapours at high temperatures (e.g. Symonds et al. (1987), Mather et al. (2012), Zelenski et al. (2013)), and show the greatest variability across this suite of samples. The Bi and Tl enrichment in the tuffsite vein of Bomb 2 (Figure 4) could be due to adsorption of these elements onto the glass shards, the result of interaction with the fluxing gas phase. Bi and Tl would be transported within the vapour phase but changing conditions upon ascent could have promoted deposition and adsorption from the gas phase (as melt-vapour partition coefficients decreased with changing conditions), the fine-grained glass shards of these veins providing a high surface area to volume ratio, ideal for adsorption. This would be analogous to metal deposition in fumaroles. Alternatively, the glass shards absorbed metals into their silicate melt structure during vein sintering and compaction; or have higher

Bi and Tl concentrations suggesting tapping of deeper, less degassed melts. Distinguishing between adsorption and absorption is beyond the scope of the methods of this paper.

Bi is also enriched in the vein of Bomb 3, but Tl is depleted (Figure 4). The apparent depletion of Tl within this vein component is due to the enrichment of Tl in the vesiculated host with respect to all other samples. The elongated and connected vesicles in this highly sheared sample suggest open channels for gas flow were present prior to tuffsite formation. Adsorption of Tl onto the channel walls during fluxing could account for its higher than average concentration, and thus lower vein-host ratio. Bi is much higher in concentration in this sample than all others from Cordón Caulle as well, supporting the theory of gas adsorption in the host component of this sample. Alternatively, the sample has lost less Tl and Bi through degassing than other samples, pointing to a larger-scale control on concentrations of volatiles preserved than individual fracture-degassing events.

The vein within Bomb 4 (Figure 4) is depleted in Tl (Bi is similar to the host), suggesting this later vein tapped a more degassed source or that conditions within the vein resulted in scavenging of metals and not metal deposition. Cd, In and Pb depletions are observed in this vein only. Depletions would suggest the system either progressively degassed over time, with earlier veins tapping gas-rich melts and later veins tapping more gas-depleted melts, or conditions changed such that earlier veins underwent metal deposition whilst later veins underwent scavenging.

In each of these cases, the affinity of both Bi and Tl for a gas phase and the textural association of the enrichments and depletions with gas pathways suggest that interactions between melt and fluxing gas was the driver for the preserved heterogeneity. However, the processes responsible remain unclear pending detailed studies on the behaviour of these elements under similar conditions. In-situ studies into Tl and Bi variation could be key to understanding the complex degassing history and Cordón Caulle.

#### **4.1.3 Why is there a disparity between the isotope and trace element signatures?**

As discussed in Section 1.2,  $^{210}\text{Pb}$ - $^{226}\text{Ra}$  disequilibria and trace element heterogeneity can be induced by degassing of a magma before and during an eruption. At both Cordón Caulle and Chaitén there is little evidence of degassing preserved in the isotope record but trace element variations in tuffisite veins at both localities do provide evidence for degassing. One key parameter for a chemical signature of degassing to be preserved is time.  $^{210}\text{Pb}$  deficits can only be formed over months to years of continuous degassing because of the need for continuous extraction of  $^{222}\text{Rn}$  from the system (Gauthier and Condomines, 1999).  $^{210}\text{Pb}$  excesses can be formed in less time, with weeks to months of gas fluxing required to transfer  $^{222}\text{Rn}$  from one location to another, and for it to then decay to  $^{210}\text{Pb}$  (Condomines et al., 2010). The timing required to generate an excess is also dependent on the mass of magma Rn is being removed from and redistributed into. If the ratio is large then less time is required to generate an excess, and we address this within the context of tuffisite veins in Section 4.2. However, trace element heterogeneity induced by degassing is a function of the characteristic diffusivities of elements in silicate melts and their vapour-melt partition coefficients and not by decay, thus they require only minutes to hours to generate sub-mm scale heterogeneity in



tuffisite vein material (MacKenzie and Canil, 2008, Berlo et al., 2013). The preservation of degassing signatures in trace elements at Chaitén and Cordón Caulle but not in isotopes suggests that individual degassing events through fractures were transient (not longer than days at a time), otherwise we would expect to see preserved signatures in both trace elements and isotopes. Furthermore, this places limits on the mass of magma that is being degassed through these channels.

#### 4.2 Why are no $^{210}\text{Pb}$ excesses preserved in veins?

The redistribution or streaming of gas (containing  $^{222}\text{Rn}$ ) through a system can result in  $^{210}\text{Pb}$  excesses. Therefore, if a fracture or tuffisite vein underwent sufficient gas streaming over time it would be expected to have a  $^{210}\text{Pb}$  excess.  $^{210}\text{Pb}$  that has decayed from volatile  $^{222}\text{Rn}$ , concentrated within the gas phase, would be resorbed by melt particles within the fracture (Lambert et al., 1985). However, despite evidence for gas streaming (e.g. metal enrichments and clastic textures), no vein material from Cordón Caulle or Chaitén has preserved a significant  $(^{210}\text{Pb})_0$  excess. We adapt the model from Condomines et al. (2010) to explain why no excesses have been preserved in veins at either volcano and which conditions could potentially form excesses at other eruptions.

Condomines et al. (2010) numerically modelled how  $^{210}\text{Pb}$  excesses ( $^{210}\text{Pb}/^{226}\text{Ra} > 1$ ) can be derived from the accumulation of  $^{222}\text{Rn}$  (and its subsequent decay to  $^{210}\text{Pb}$ ). Their model accounts for the mass ratio ( $R$ ) of the magma degassing cells losing gas ( $M_d$ ) and accumulating Rn ( $M_a$ ); the fraction of Rn extracted from the degassing cell ( $f$ ) and from the

accumulating cell ( $f'$ ); as well as the volatile content of the undegassed magma ( $\alpha$ ) and the magma's residence time in the degassing cell ( $\tau$ ) (Figure 5). We present a model adapted from Condomines et al. (2010) and the original differential decay equations as derived by Bateman (1910). The model constrains the mass ratio required to generate an excess of  $^{210}\text{Pb}$  in the vein given a degassing event of  $X$  hours. It is divided into two parts. Part One calculates the evolution of ( $^{210}\text{Pb}$ ), ( $^{222}\text{Rn}$ ) and ( $^{226}\text{Ra}$ ) with time while the fracture is open and  $^{222}\text{Rn}$  is being redistributed from the degassing cell to the fracture via gas streaming (Figure 5). Part Two allows for the assessment of the final ( $^{210}\text{Pb}/^{226}\text{Ra}$ ) of the bulk fracture assuming no further loss of  $^{222}\text{Rn}$  or  $^{210}\text{Pb}$  following closure and sealing of the vein. Only re-equilibration and decay of the nuclides present at the time of vein closure occurs during this time.

#### 4.2.1 Part One: Radon Redistribution during fracturing and gas streaming

Following the approach of Condomines et al. (2010), the  $^{222}\text{Rn}$  variation per unit time in the fracture is given by:

$$\frac{d(\text{Rn})_a}{dt} = \frac{1}{M_a} [(\phi_{\text{Rn}}^{\text{in}}) - (\phi_{\text{Rn}}^{\text{out}})] + \lambda_{\text{Rn}}(\text{Ra})_a - \lambda_{\text{Rn}}(\text{Rn})_a \quad (1)$$

Where  $\phi_{\text{Rn}}^{\text{in}}$  and  $\phi_{\text{Rn}}^{\text{out}}$  are defined as the flux of Rn in and out of the accumulating cell, in this case the fracture preserved as the tuffisite vein.  $M_a$  is the mass of the tuffisite vein;  $\lambda_{\text{Rn}}$  is the decay constant of Rn; and  $(\text{Ra})_a$  and  $(\text{Rn})_a$  are the  $^{226}\text{Ra}$  and  $^{222}\text{Rn}$  activities of the tuffisite material respectively. The parameters  $f$  and  $f'$  denote the fraction of Rn effectively extracted from the degassing magma cell, and accumulating magma cell respectively:

$$f = \frac{(\phi_{Rn}^{in})}{[\lambda_{Rn}M_d + (1-\alpha)\phi_o](Ra)_d} \quad (2)$$

$$f' = \frac{(\phi_{Rn}^{out})}{[\lambda_{Rn}M_a(Ra)_a + (\phi_{Rn}^{in})]} = \frac{(\phi_{Rn}^{out})}{[\lambda_{Rn}M_a(Ra)_a + f(\lambda_{Rn}M_d + (1-\alpha)\phi_o)(Ra)_d]} \quad (3)$$

Where  $M_d$  is the mass of the degassing cell,  $\phi_o$  is the influx of undegassed magma into the degassing reservoir,  $\alpha$  is the volatile content of the undegassed magma, and  $(Ra)_d$  is the  $^{226}\text{Ra}$  activity of the degassing cell (see Fig. 5). Condomines et al. (2010) simplify their equations because  $(Rn/Ra)_a$  will reach a steady state after several weeks as Rn, and other intermediary nuclides, are in secular equilibrium with Ra. This is an assumption we are unable to make as the fractures are only open on the order of hours to days (Castro et al., 2012, Berlo et al., 2013). Thus we combine the above equations and simplify by introducing the parameters residence time,  $\tau = M_d/\phi_o$ , and mass ratio,  $R = M_d/M_a$ , as suggested by Condomines et al. (2010), and restricting our model to  $(Ra)_a = (Ra)_d$ . This is a valid assumption as ( $^{226}\text{Ra}$ ) is immobile, does not partition into a gas phase (Lambert et al., 1985), and these systems show no significant Ra variation over time (see Section 3, Fig. 2). The changing ( $^{222}\text{Rn}$ ) with time can then be represented by:

$$\frac{d(Rn)_a}{dt} = \lambda_{Rn}(Ra)_a C - \lambda_{Rn}(Rn)_a \quad (4)$$

Where:

$$C = (1 - f') \left[ 1 + fR \left[ 1 + \frac{(1-\alpha)}{\lambda_{Rn}\tau} \right] \right]. \quad (5)$$

This modified equation takes into account the additional  $^{222}\text{Rn}$  from the decay of  $^{226}\text{Ra}$  in the degassing cell, the  $^{222}\text{Rn}$  lost from the fracture, and  $^{222}\text{Rn}$  that comes from the decay of  $^{226}\text{Ra}$  in the tuffisite material within the fracture. Appendix B provides further details on the derivation of this equation and equations underpinning both parts of the model presented.

The model uses the complete solutions to the decay equations, as described by Bateman (1910), assuming that  $^{226}\text{Ra}$  and its products,  $^{222}\text{Rn}$  and  $^{210}\text{Pb}$ , start in secular equilibrium. The additional  $^{222}\text{Rn}$  is accounted for in the equations for both ( $^{222}\text{Rn}$ ) and ( $^{210}\text{Pb}$ ) variation with time. There are several, short-lived intermediate nuclides between  $^{222}\text{Rn}$  and  $^{210}\text{Pb}$  that we have not included within the model. We assume that  $^{218}\text{Po}$  ( $t_{1/2} \sim 3.05$  mins) and  $^{214}\text{Po}$  ( $t_{1/2} \sim 1.64 \times 10^{-4}$  s) are in secular equilibrium the whole time due to their short half-lives and can be ignored. If the fracture is open for  $< 2 \frac{1}{2}$  hours then  $^{214}\text{Pb}$  and  $^{214}\text{Bi}$  stay trapped and do not need to be considered separately as  $^{214}\text{Pb}$  would be resorbed into melt particles, and  $^{214}\text{Bi}$  would stay volatile with Rn. If the vein is open longer, they are in secular equilibrium with  $^{222}\text{Rn}$ . Finally, we assume negligible Rn flux from vein walls when compared to contribution from depth, due to slow Rn diffusion (Gauthier et al., 1999), thus R represents purely the mass ratio between the fracture and degassing cell. The model numerically calculates the activities of Pb, Rn and Ra and the activity ratios ( $^{222}\text{Rn}/^{226}\text{Ra}$ ) and ( $^{210}\text{Pb}/^{226}\text{Ra}$ ) for a fracture open between 0 and 36 hours (t), a timespan that applies to veins at both these and other volcanoes such as Torfajökull (Iceland) and Lipari (Italy) (Cabrera et al., 2010, Castro et al., 2012, Berlo et al., 2013). The parameters inputted into the calculations representing Rn extraction from the degassing chamber (f) and the fracture (f') vary from 0 to 1, and R (the mass ratio,  $M_d/M_a$ ) varies from 0.1 to  $1 \times 10^6$  to provide a full range of potential scenarios.

#### 4.2.2 Part Two: Vein Closure and Subsequent Decay

Eventually, radon gas transport will cease because particles within the vein will have sintered to the point at which the system becomes closed to gases (Farquharson et al., 2017). Excess Rn trapped within the isolated porosity of the vein will decay to Pb and be reintroduced into the melt (Condomines et al., 2010). Part two of the model calculates the decay of  $^{210}\text{Pb}$ ,  $^{222}\text{Rn}$  and  $^{226}\text{Ra}$  and activity ratios Rn/Ra and Pb/Ra for scenarios with varying  $f$ ,  $f'$ ,  $R$  and  $t$  values. After ~50 days the activity of  $^{222}\text{Rn}$  has returned to within error of its original activity,  $^{210}\text{Pb}$  and  $^{222}\text{Rn}$  are in secular equilibrium, and  $(^{210}\text{Pb}/^{226}\text{Ra})$  has reached its maximum. Contoured plots generated show the  $R$  value required, for given  $f'$  and  $\tau$  values, to generate  $(^{210}\text{Pb}/^{226}\text{Ra}) \sim 1.10$  (a ratio that deviates from secular equilibrium by more than analytical error). This is for a fracture open over a range of timescales, e.g. Figure 6 where  $\tau = 0.019$ ,  $f = 1$ ,  $f' = 0.5$  and  $t = 0\text{--}15$  hours.

#### 4.2.3 Applying the model: Chaitén

Previous studies on tuffisite veins from Chaitén make this a prime case study to test this model. Diffusion modelling of  $\text{H}_2\text{O}$  towards fractures in bombs from the 2008 Chaitén eruption suggests fractures are open on the order of hours (Castro et al., 2012). We assume the degassing cell is an isolated parcel of magma, isolated prior to and upon ascent within the conduit. As the system becomes closed,  $\tau \rightarrow \infty$ . Appendix C summarises the effect of varying  $\tau$  on the required  $R$  values, with negligible differences in required  $R$  when  $\tau > 1$ . Here we use a  $\tau$  value of 0.019 (equivalent to the cell being isolated for 1 week before being degassed by the fracture). Castro and Dingwell (2009) indicate that magma at depth at Chaitén contained <4 wt. %  $\text{H}_2\text{O}$  thus we choose  $\alpha = 0.04$ , this is the volatile content of the undegassed magma that is ultimately exsolved. Sensitivity analysis indicates that variation of  $\alpha$  has a negligible

impact on the final values of the model. Assuming complete extraction of Rn from the degassing chamber ( $f = 1$ ) for a fracture open for 7.5 hours, mass ratios ( $R = M_d/M_a$ ) of ~3000-9000 are required to generate an activity ratio of ( $^{210}\text{Pb}/^{226}\text{Ra}$ ) ~1.10 (the minimum  $^{210}\text{Pb}$  excess that would be outside of error) depending on the amount of Rn extracted from the vein to the surface ( $f^* = 0.25-0.75$ ). Here an  $f^*$  value of 0.25 implies 25 % of available Rn is extracted out of the vein during the time the vein is open. R increases fourfold from 4,500 to 20,000 as fracture lifespan decreases from ~7.5 hours to ~1.6 hours (assuming  $f = 1$ ,  $f^* = 0.5$  and  $\tau = 0.019$ , see Figure 6). These values would increase if  $f < 1$ , therefore these are minimum values. The model sensitivity to varying  $f$  values is discussed in Appendix C. The model provides an estimate on the size of a melt pocket that can be degassed by a fracture during its lifetime. As an example, a sheet-shaped vein with a 5 cm aperture, 6-50 m wide, with 150 m of vertical length, would have a  $M_a$  between  $9.3 \times 10^4$  and  $7.8 \times 10^5$  kg assuming a bulk density of  $2070 \text{ kg/m}^3$  (Saubin et al., 2016). This would correspond to a degassing cell mass ( $M_d$ ) between  $4.7 \times 10^8$  and  $3.9 \times 10^9$  kg (or  $\sim 2 \times 10^5$ - $1.7 \times 10^6 \text{ m}^3$  of magma, assuming a density of  $2281 \text{ kg/m}^3$ ) at  $R \sim 5,000$ . Geometrically, this is equivalent to a single vein efficiently degassing a cylindrical parcel of magma ~350 m in length with a radius between 14 and 40 m, within a lifespan of several hours.  $\text{H}_2\text{O}$  cannot diffuse in a dense melt over a metre length scale on these timescales (e.g. Castro et al. (2012)). Furthermore, these calculations highlight the implausible cylinder radii required for wider veins (e.g. 40 m), that suggest they were degassing a melt wider than the conduit itself. For this unlikely scenario to occur the magma being degassed would require an extensively connected bubble network across its length and width for gas to segregate into and move these distances before then outgassing through the fracture. Thus, the model highlights that disequilibria, induced within a single fracture and gas fluxing event, are highly unlikely to be preserved in veins open for such a short a period of time.

#### 4.2.4 Applying the model: Other Systems

The model outputs imply that if veins are open long enough, >1 day, it could be possible to generate a small  $^{210}\text{Pb}$  excess under favourable conditions (Figure 6, Appendix C). For this model to be applied to other systems fracture opening timescales are required, via measurement or estimation. This can be done via diffusion studies, e.g. Castro et al. (2012) or via visual observation, e.g. Schipper et al. (2013), if the assumption is made that vents or sub-vents are the surface manifestation of gas fluxing through fractures at depth. Once a time estimate is known, isotope disequilibria will aid in constraining the mass of magma being degassed by fractures during those events. Tuffisite veins in volcanic centres, such as those in a ~70 ka dissected conduit at Torfajökull in Iceland, show evidence of being longer-lived (Berlo et al., 2013). However, isotope systematics dictate that this model can be only used only recent eruptions, as all  $^{210}\text{Pb}$  disequilibria will decay away after ~120 years (~5 half-lives of  $^{210}\text{Pb}$ ).

#### 4.3 Other processes inducing tuffisite vein trace element heterogeneity

Some of the chemical heterogeneity in the tuffisite veins are in elements that are not commonly associated with degassing because of their immobility, non-volatility, and general preference for mineral phases (e.g. Group 1 and Group 3 elements). Thus, degassing is unlikely to be the cause of the heterogeneity. At Chaitén HFSEs and U are depleted in the Bomb A vein sub-samples with respect to the host, and at Cordón Caulle many major

elements and transition elements (e.g. Mg, Sr, and V) are depleted in the three separate veins with respect to their hosts. These variations though can be explained through different physical processes than degassing as discussed below and highlight the importance of analysing a wide suite of elements with varying properties.

## Chaitén

The biggest compositional variations in the Chaitén samples are within the vein matrices and Banded Clast components of Bomb A (Figure 3). As previously mentioned, the Banded Clast is interpreted as non-juvenile material (Saubin et al., 2016). Group 3 elements (HFSEs and U) are generally highly incompatible in many mineral phases, but are commonly found in elevated concentrations in the refractory mineral zircon (Belousova et al., 2002). Zr, Hf and Nb are the most depleted elements in the Banded Clast (excluding the volatile elements discussed in Section 4.1), followed by U, Ta, the heavy REEs (Dy to Lu) and Y. Apparent partition coefficients calculated from the observed deficits are consistent with that of zircon crystallisation ( $D_{Zr} > D_{Hf} > D_U > D_{HREEs} \sim D_Y$ , Fujimaki (1986), Thomas (2003)). This would require these clasts to have undergone a different cooling history to the zircon undersaturated, main 2008 melt (Boehnke et al., 2013). We propose that the Banded Clast represents a previous rhyolitic dome, which would have cooled more slowly through the zircon saturation temperature ( $\sim 712^\circ\text{C}$  based on calculations by Boehnke et al. (2013) assuming a similar composition to the 2008 melt), allowing for the formation of micron-sized zircons. This would explain why the zircon signature is only found in these clasts and not in the juvenile melt of Bombs A and B.



The elemental composition of the Banded Clast will affect the vein sub-samples from Bomb A as the clasts are a sizable component of the vein's textural make-up. The Banded Clast analysed is ~1 cm in across, however most clasts of this type range from ~0.1 to ~8 mm in size (Saubin et al., 2016). Saubin et al. (2016) report that banded clasts accounted for  $42 \pm 3$  % of this tuffisite vein, with dense clasts accounting for  $35 \pm 3$  % and pale vesicular clasts  $22 \pm 4$  %. Using this information, we construct a simple three component mixing model, assuming this component ratio (42:35:22), to predict the concentrations of elements in the tuffisite vein, and account for the apparent elemental depletions within the Vein Matrix and Matrix & Clasts sub-samples (Fig. S.1). These sub-samples are depleted in HFSEs, U, and some volatiles (Li, Mo, Bi) but to a lesser extent than the Banded Clast (see Section 3.3, Fig. 3). Dense clasts are assumed to have a composition identical to the host, the banded clasts' composition is known, and we use average element concentrations for the pumice clasts from Berlo et al. (2013) for the three-component model. Certain elements (Yb, Y, Zr, Nb, W, Cs, Ag, Cd and Bi) were not analysed by Berlo et al. (2013) so their concentration in the pumice clasts are assumed to be the same as that of the host. This is a valid assumption as Saubin et al. (2016) state these clasts fragmented deep in the system and were brought up into the vein, suggesting they are part of the 2008 juvenile melt that is chemically well constrained (see Section 3.3). This reduces the 3-component mixing model to a two-component mixing model between Host (~57 %) and Banded Clast (~42 %). These models reproduce, within error, observed depletions in Figure 3 (Fig. S.1) with exception of Nb that is just outside of error, Cu (Matrix sub-sample), Mo and Bi (in both sub-samples). The underestimation of Cu, Sb, Mo and Bi concentrations by the model suggests that these elements have been added to the vein, supporting the theory of gas streaming discussed in Section 4.1 and by Berlo et al. (2013). Thus, the depletions in the more immobile elements, and most volatile elements,

within the vein at Chaitén are due to mixing and bulk analysis of clasts, with subtle compositional differences, that have been transported along with the gas phase. The compositions of these individual clasts represent their histories (degassing, crystallisation etc.) prior to entrainment within the tuffisite vein. This mixing of three clast types with subtly different compositions has likely masked the enrichment of certain volatile elements (Cu, Mo and Bi) that have been fluxed through with the gas phase and adsorbed onto the clast surfaces within the vein.

### **Cordón Caulle**

Three tuffisite samples show similar trace element ratios when normalised to their respective hosts (Figure 4). Anomalies in the Group 1 elements are unlikely to result from degassing but could be the result of preferential fracturing and transportation of glass over the phenocryst assemblage (plagioclase, orthopyroxene, clinopyroxene, Fe-Ti oxides and accessory apatite) during fragmentation. Horwell et al. (2001) found that the components of different size fractions of the pyroclastic flow deposits at Soufrière Hills volcano were altered due to physical processes. Larger size fractions are found to be phenocryst-enriched whilst the finer size fractions of the concurrent ash fall deposits are glass-enriched and this fractionation is reflected in the deposits' geochemistry. Laser ablation analysis of volcanic glass from Cordón Caulle (Paisley et al., in prep.) indicates these Group 1 elements (e.g. V, Mg, P, Sr, Mn) are lower in concentration than the bulk (crystals + glass) analyses described in Section 3. Furthermore, petrographic studies on other tuffisite samples from Cordón Caulle show that fine-grained laminae within tuffisite veins are often devoid of crystals or fragments when compared to coarser beds (Paisley et al., in prep.). Rare phenocrysts are hosted within clasts

with complex banded textures, in coarse-grained beds, or are in the form of microlites within glass shards of different sizes that grew upon ascent. Finally, the crystal content of the Cordón Caulle deposits is relatively low (~5 %), and crystals are commonly found as glomerocrysts (Castro et al., 2013a), which are not widely observed in the tuffisite veins. Thus, we suggest that the preferential fracturing and transport of glass through tuffisites is the cause in the depletions of these elements within veins. This discovery has implications regarding the formation of source material for tuffisites and whether the pressurisation and fragmentation of crystal-poor, vesicular melt at depth results in the preferential movement of the glass-rich shards through propagating fracture networks.

#### 4.4 Isotopic outliers: Samples not in secular equilibrium

Although the majority of samples at both volcanoes are within secular equilibrium there are notable outliers that can be addressed.

##### Chaitén

Bomb B (Exterior) from Chaitén is not in secular equilibrium. Bomb B (Exterior) has a  $(^{226}\text{Ra}) = 42.01 \pm 3.46 \text{ Bq/kg}$ , a value within error of its predicted activity based on its U concentration ( $3.41 \pm 0.19 \text{ ppm}$ ). In contrast the Bomb B (Interior) has a lower  $(^{226}\text{Ra})$  than predicted but a  $^{210}\text{Pb}$ - $^{226}\text{Ra}$  ratio within secular equilibrium. Degassing is unlikely the cause of this deficit, as Ra is not a volatile element. Ra is highly incompatible too and Ra partition

coefficients are usually smaller than those of Pb. However, an explanation that fractional crystallisation could have played a role in this deficit is implausible as textures show negligible in-situ microlite growth within the bomb. Therefore, the  $^{226}\text{Ra}$  depletion is not readily explained.

### Cordón Caulle

The tuffisite vein within Bomb 4, representing later hybrid activity, is the only sub-sample to show internal isotope variation with  $(^{210}\text{Pb}/^{226}\text{Ra})_o = 0.90 \pm 0.02$  (Figure 1), and its origin can be decoded using  $(^{210}\text{Pb})_o/\text{Pb}$ . Significant degassing ( $^{222}\text{Rn}$  removal) or fluxing ( $^{222}\text{Rn}$  addition) will decrease or increase this ratio respectively, as common lead is not influenced by this process (Turner et al., 2004). The vein component of Bomb 4 has a  $(^{210}\text{Pb})_o/\text{Pb} = 0.083 \pm 0.002$ , similar to other Cordón Caulle samples, and  $(^{210}\text{Pb})_o/\text{Pb} \sim 0.086$ . The vein is depleted in total Pb compared to the host (Figure 4), with a ratio of  $\sim 0.9$ , and has a  $(^{210}\text{Pb})_{\text{vein}}/(^{210}\text{Pb})_{\text{host}} \sim 0.94$ . In comparison, other veins have a  $(^{210}\text{Pb})_{\text{vein}}/(^{210}\text{Pb})_{\text{host}}$  within error of 1. Thus, the vein's reduced  $(^{210}\text{Pb})_o$  may result from extraction of total lead (all isotopes, not only  $^{210}\text{Pb}$ ) during a later degassing event, e.g. during fracturing and vein formation, and not prior degassing. Only one sample, Bomb 5, has a  $^{210}\text{Pb}$  excess relative to  $^{226}\text{Ra}$ ,  $(^{210}\text{Pb}/^{226}\text{Ra})_o = 1.19 \pm 0.17$  (Figure 2). Its  $(^{210}\text{Pb})_o/\text{Pb} = 0.107 \pm 0.006$  which is significantly higher than the average and could indicate abundant gas streaming. Adsorption of Po and Pb from the outgassing vapour by the vesicular sample within the vent would account for its elevated ratios.

#### 4.5 Why is degassing preserved differently at Chaitén and Cordon Caulle?

Trace elements have recorded a clear signal of degassing. Chaitén veins have volatile trace element enrichments whilst Cordon Caulle veins have some enrichments but also have depletions (e.g. Bomb 4). This initially appears counterintuitive as the veins at both volcanoes act as gas flow pathways whilst the fractures are open and thus similar gas flow signatures might be expected. We suggest that the difference in the depth of upper conduit fracturing at the two volcanoes can explain the contrasting signatures. Fracturing at Chaitén is thought to range from the surface to a depth of ~500 m with extensive connectivity (Castro et al., 2014, Saubin et al., 2016, Farquharson et al., 2017). In contrast, at Cordon Caulle extensive fracturing has been shown to occur in the near surface environment (<20 m), only extending down to ~200 m (Schipper et al., 2013, Castro et al., 2016). Farquharson et al. (2017) suggest that veins will undergo different degassing regimes depending on the relative timescales of three processes: fluid flow ( $\tau_{Da}$ ), porosity reduction (i.e. compaction,  $\tau_C$ ); and volatile exchange with the sintering melt ( $\tau_D$ ). Providing  $\tau_C > \tau_{Da}$ , veins sit in an outgassing regime as pore fluid pressures continually equilibrate as compaction occurs. If  $\tau_{Da} > \tau_C$  then pore pressure equilibrium is not maintained, and veins will undergo either volatile exchange with the melt ( $\tau_{Da} > \tau_C > \tau_D$ ) or pore pressure increases ( $\tau_{Da} > \tau_D > \tau_C$ ) which results in favourable conditions for explosive fragmentation. This is summarised by a critical permeability threshold ( $k_{cr}$ ). If fracture permeability ( $k_f$ ) is less than or equal to  $k_{cr}$  it implies pore fluid pressures will increase and potentially result in explosive fragmentation. Although initially  $k_f$  is high, compaction and sintering reduces this value with time, tending towards the magma's initial permeability ( $k_o$ ) (Kolzenburg et al., 2012, Farquharson et al., 2017).

In shallower environments Farquharson et al. (2017) predict that fractures would sit in an outgassing regime as lower pressures result in lower  $k_{cr}$  values and longer  $\tau_D$  times. Fractures remain open longer, before compaction reduces their permeability so that  $k_f < k_{cr}$ , and more time would be required for volatiles to diffusively resorb into the sintering vein particles and element enrichment occurring. This matches observations from Cordon Caulle. Low  $H_2O$  groundmass concentrations and oxidation suggest fracturing and quenching are occurring at shallower depths than Chaitén (<200 m vs <500 m), and there is direct outgassing to the atmosphere from certain fractures (Schipper et al., 2013, Castro et al., 2014, Castro et al., 2016). We observe minimal elemental enrichments (with the exception of Bi) suggesting less interaction between particles and the gas phase (due to longer  $\tau_D$ ). Furthermore, as stated by Farquharson et al. (2017) Cordon Caulle has a relatively high calculated  $k_{cr}$  which would result in frequent pressure build ups (when  $k_f < k_{cr}$ ), incomplete sintering (as observed in Figure 1) and frequent explosions (as observed by Schipper et al. (2013)). Thus, elemental enrichments in tuffisite veins in early Cordon Caulle bombs are unlikely the result of diffusive absorption of volatiles but it is unclear if adsorption processes would occur under these conditions. Thus, Tl and Bi enrichments could be due to shards having higher concentrations prior to entrainment in the vein (a richer Tl and Bi source melt) or elemental adsorption. Depletions in the Bomb 4 vein could be the result of diffusion out of glass shards (element scavenging as observed at Torfajökull by Berlo et al. (2013)), which could be resolved by in situ analysis. At Chaitén bombs are excavated from deeper (Castro et al., 2014) and veins record vertical clast transport over hundreds of metres (Berlo et al., 2013, Saubin et al., 2016). Such conditions would result in higher  $k_{cr}$  values and shorter  $\tau_D$  times than Cordon Caulle, and be ideal for volatile exchange (Farquharson et al., 2017). Veins equilibrate with trapped gases in isolated pockets as particles sinter, exchanging volatiles and resulting in enrichments (see Figure 3), before entering the pore pressure increase regime ( $\tau_{Da}$

$> \tau_D > \tau_C$ ) where pressure build-up results in fragmentation and bomb ejection. Differing gas compositions and eruptive temperatures would also influence the exchange of volatile species, as well as which elements are available to exchange.

Studying trace elemental variation in tuffisite veins, brecciated conduit margins, and shear zones at other volcanoes would aid in understanding the depth to which these channels are open, available for degassing, and their role in the trace metal budget of eruptions. This would be a particularly useful approach to look at near-surface degassing processes occurring during fracturing and dome formation, where volatiles such as  $H_2O$  would have already been largely lost. This study also has implications in the study of vapours as a method of metal transport, e.g. Williams-Jones and Heinrich (2005) and van Hinsberg et al. (2016), highlighting that deeper veins forming during volcanic activity appear to show more metal enrichments than their shallower counterparts.

## 5. Conclusions

Our study of tuffisite veins from the two recent rhyolitic eruptions provides an insight into how syn-eruptive physical processes, such as degassing, are geochemically preserved. Although both Chaitén and Cordon Caulle have undergone gas streaming it is recorded differently in trace elements and isotopes. Cu enrichments record gas streaming and volatile exchange at Chaitén. At Cordon Caulle trace element depletions (e.g. Cd, In, Pb and Tl) indicate degassing during fracturing events. However, no systematic evidence of degassing has been preserved in the isotope record at either volcano, suggesting degassing events were

of insufficient duration and efficiency for the formation of disequilibria between  $^{210}\text{Pb}$  and  $^{226}\text{Ra}$ . The lack of  $^{210}\text{Pb}$  excesses preserved in veins from both eruptions allows us to calculate an upper limit on the magma mass being degassed by individual tuffisite veins during these eruptions. We have also shown that other physical processes, such as the preferential movement of glass over crystals, can be chemically preserved in tuffisites.

This study reinforces the idea that trace elements are valuable tools for understanding syn-eruptive physical processes, particularly at systems with erupted deposits depleted in major volatiles such as  $\text{H}_2\text{O}$  (e.g. Cordon Caulle). By analysing for a wide suite of elements, both non-volatile and volatile, it is possible to distinguish between degassing processes and physical processes redistributing clasts, crystals and glass during fracturing and vein formation. It is also possible to discriminate between early degassing events (preserved within clasts in veins) and syn-fracture degassing by analysing the different components of individual tuffisites. This method of analysis could be easily applied to other volcanoes to assess the role of fracturing in degassing in different volcanic environments and be extended to the micron-scale using in situ methods.

## 6. Acknowledgements

RP would like to thank Alex Corgne, Nicolas Vergara Pontigo and Felipe Ignacio P. Gallardo for assistance in the field; Anna Jung and André Poirier for instrument assistance; and Vincent van Hinsberg for constructive analytical advice. The authors appreciate constructive comments on an earlier manuscript from Jacqueline Owen, Jamie Farquharson, and from an



anonymous reviewer and the rapid and thorough reviews on this manuscript from Fabian Wadsworth and an anonymous reviewer. RP was supported by travel and research grants from the Mineralogical Association of Canada and the Geological Society of America. This work is supported by a NSERC Discovery Grant to KB. Certain samples from Cordón Caulle (Flow 1, Bomb 1 and Bomb 2) and Chaitén (Bombs A and B) were collected during fieldwork supported by the European Research Council under the European Union's Seventh Framework Programme FP7/2007-2013 grant agreement No 307356 to KB. HT and KB would like to thank Jon Castro, Ian Schipper, Fabian Wadsworth, Amy Chadderton and Peter Sammonds for their time and assistance in the field. HT is supported by a Royal Society University Research Fellowship and thanks Sports Centre and Facilities staff at Lancaster University for assistance.

Declarations of Interest: none

## 7. References

- AMIGO, A., LARA, L. E. & SMITH, V. C. 2013. Holocene record of large explosive eruptions from Chaitén and Michinmahuida Volcanoes, Chile. *Andean Geology*, 40, 227-248.
- BATEMAN, H. The solution of a system of differential equations occurring in the theory of radioactive transformations. *Proc. Cambridge Philos. Soc.*, 1910. 423-427.
- BELOUSOVA, E., GRIFFIN, W., O'REILLY, S. Y. & FISHER, N. 2002. Igneous zircon: trace element composition as an indicator of source rock type. *Contributions to Mineralogy and Petrology*, 143, 602-622.
- BERLO, K., TUFFEN, H., SMITH, V. C., CASTRO, J. M., PYLE, D. M., MATHER, T. A. & GERAKE, K. 2013. Element variations in rhyolitic magma resulting from gas transport. *Geochimica et Cosmochimica Acta*, 121, 436-451.
- BERLO, K. & TURNER, S. 2010.  $^{210}\text{Pb}$ – $^{226}\text{Ra}$  disequilibria in volcanic rocks. *Earth and Planetary Science Letters*, 296, 155-164.
- BERLO, K., TURNER, S., BLUNDY, J., BLACK, S. & HAWKESWORTH, C. 2006. Tracing pre-eruptive magma degassing using ( $^{210}\text{Pb}/^{226}\text{Ra}$ ) disequilibria in the volcanic deposits of the 1980–1986 eruption of Mount St. Helens. *Earth and Planetary Science Letters*, 249, 337-349.
- BOEHNKE, P., WATSON, E. B., TRAIL, D., HARRISON, T. M. & SCHMITT, A. K. 2013. Zircon saturation re-revisited. *Chemical Geology*, 351, 324-334.
- BOURDON, B., GEOCHEMICAL, S. & MINERALOGICAL SOCIETY OF, A. 2003. *Uranium-series geochemistry*, [St. Louis, Mo.]; Washington, DC, Geochemical Society ; Mineralogical Society of America.

- CABRERA, A., WEINBERG, R. F., WRIGHT, H. M. N., ZLOTNIK, S. & CAS, R. A. F. 2010. Melt fracturing and healing: A mechanism for degassing and origin of silicic obsidian. *Geology*, 39, 67-70.
- CASTRO, J. M., BINDEMAN, I. N., TUFFEN, H. & IAN SCHIPPER, C. 2014. Explosive origin of silicic lava: Textural and  $\delta D-H_2O$  evidence for pyroclastic degassing during rhyolite effusion. *Earth and Planetary Science Letters*, 405, 52-61.
- CASTRO, J. M., CORDONNIER, B., SCHIPPER, C. I., TUFFEN, H., BAUMANN, T. S. & FEISEL, Y. 2016. Rapid laccolith intrusion driven by explosive volcanic eruption. *Nat Commun*, 7, 13585.
- CASTRO, J. M., CORDONNIER, B., TUFFEN, H., TOBIN, M. J., PUSKAR, L., MARTIN, M. C. & BECHTEL, H. A. 2012. The role of melt-fracture degassing in defusing explosive rhyolite eruptions at volcán Chaitén. *Earth and Planetary Science Letters*, 333-334, 63-69.
- CASTRO, J. M. & DINGWELL, D. B. 2009. Rapid ascent of rhyolitic magma at Chaiten volcano, Chile. *Nature*, 461, 780-3.
- CASTRO, J. M., SCHIPPER, C. I., MUELLER, S. P., MILITZER, A. S., AMIGO, A., PAREJAS, C. S. & JACOB, D. 2013a. Storage and eruption of near-liquidus rhyolite magma at Cordón Caulle, Chile. *Bulletin of Volcanology*, 75:202.
- CASTRO, J. M., SCHIPPER, C. I., TUFFEN, H., JAMES, M. R. & MILITZER, A. S. 2013b. Reassembling a volcanic conduit using bombs at Cordón Caulle, Chile. *IAVCEI 2013 Scientific Assembly*. Kagoshima, Japan.
- CHURAKOV, S. V., TKACHENKO, S. I., KORZHINSKII, M. A., BOCHARNIKOV, R. E. & KIRILL, S. 2000. *Evolution of composition of high-temperature fumarolic gases from Kudryavy Volcano, Iturup, Kuril Islands: The thermodynamic modeling*.

- CONDOMINES, M., SIGMARSSON, O. & GAUTHIER, P. J. 2010. A simple model of  $^{222}\text{Rn}$  accumulation leading to  $^{210}\text{Pb}$  excesses in volcanic rocks. *Earth and Planetary Science Letters*, 293, 331-338.
- CUNNINGHAM, H. S., TURNER, S. P., PATIA, H., WYSOCZANSKI, R., NICHOLS, A. R. L., EGGINS, S. & DOSSETO, A. 2009. ( $^{210}\text{Pb}/^{226}\text{Ra}$ ) variations during the 1994–2001 intracaldera volcanism at Rabaul Caldera. *Journal of Volcanology and Geothermal Research*, 184, 416-426.
- EDMONDS, M. 2008. New geochemical insights into volcanic degassing. *Philos Trans A Math Phys Eng Sci*, 366, 4559-79.
- EICHELBERGER, J. C., CARRIGAN, C. R., WESTRICH, H. R. & PRICE, R. H. 1986. Non-explosive silicic volcanism. *Nature*, 323, 598-602.
- FARQUHARSON, J. I., HEAP, M. J., LAVALLÉE, Y., VARLEY, N. R. & BAUD, P. 2016. Evidence for the development of permeability anisotropy in lava domes and volcanic conduits. *Journal of Volcanology and Geothermal Research*, 323, 163-185.
- FARQUHARSON, J. I., WADSWORTH, F. B., HEAP, M. J. & BAUD, P. 2017. Time-dependent permeability evolution in compacting volcanic fracture systems and implications for gas overpressure. *Journal of Volcanology and Geothermal Research*, 339, 81-97.
- FUJIMAKI, H. 1986. Partition coefficients of Hf, Zr, and REE between zircon, apatite, and liquid. *Contributions to Mineralogy and Petrology*, 94, 42-45.
- GAUTHIER, P.-J. & CONDOMINES, M. 1999.  $^{210}\text{Pb}$ – $^{226}\text{Ra}$  radioactive disequilibria in recent lavas and radon degassing: inferences on the magma chamber dynamics at Stromboli and Merapi volcanoes. *Earth and Planetary Science Letters*, 172, 111-126.
- GAUTHIER, P.-J., CONDOMINES, M. & HAMMOUDA, T. 1999. An experimental investigation of radon diffusion in an anhydrous andesitic melt at atmospheric

- pressure: implications for radon degassing from erupting magmas. *Geochimica et Cosmochimica Acta*, 63, 645-656.
- GHALEB, B., PONS-BRANCHU, E. & DESCHAMPS, P. 2004. Improved method for radium extraction from environmental samples and its analysis by thermal ionization mass spectrometry. *Journal of Analytical Atomic Spectrometry*, 19, 906-910.
- GONNERMANN, H. M. & MANGA, M. 2003. Explosive volcanism may not be an inevitable consequence of magma fragmentation. *Nature*, 426, 432-435.
- GONNERMANN, H. M. & MANGA, M. 2007. The Fluid Mechanics Inside a Volcano. *Annual Review of Fluid Mechanics*, 39, 321-356.
- HEAP, M. J., FARQUHARSON, J. I., WADSWORTH, F. B., KOLZENBURG, S. & RUSSELL, J. K. 2015. Timescales for permeability reduction and strength recovery in densifying magma. *Earth and Planetary Science Letters*, 429, 223-233.
- HEIKEN, G., WOHLLETZ, K. & EICHELBERGER, J. 1988. Fracture fillings and intrusive pyroclasts, Inyo Domes, California. *Journal of Geophysical Research*, 93.
- HINKLEY, T. K., LE CLOAREC, M. F. & LAMBERT, G. 1994. Fractionation of families of major, minor, and trace metals across the melt-vapor interface in volcanic exhalations. *Geochimica et Cosmochimica Acta*, 58, 3255-3263.
- HORWELL, C., P. BRAÑA, L., S. J. SPARKS, R., D. MURPHY, M. & HARDS, V. 2001. A geochemical investigation of fragmentation and physical fractionation in pyroclastic flows from the Soufrière Hills volcano, Montserrat. 109.
- JAUPART, C. & ALLÈGRE, C. J. 1991. Gas content, eruption rate and instabilities of eruption regime in silicic volcanoes. *Earth and Planetary Science Letters*, 102, 413-429.
- JAY, J., COSTA, F., PRITCHARD, M., LARA, L., SINGER, B. & HERRIN, J. 2014. Locating magma reservoirs using InSAR and petrology before and during the 2011–

- 2012 Cordon Caulle silicic eruption. *Earth and Planetary Science Letters*, 395, 254-266.
- KAYZAR, T. M., COOPER, K. M., REAGAN, M. K. & KENT, A. J. R. 2009. Gas transport model for the magmatic system at Mount Pinatubo, Philippines: Insights from (210Pb)/(226Ra). *Journal of Volcanology and Geothermal Research*, 181, 124-140.
- KENDRICK, J. E., LAVALLÉE, Y., VARLEY, N. R., WADSWORTH, F. B., LAMB, O. D. & VASSEUR, J. 2016. Blowing Off Steam: Tuffisite Formation As a Regulator for Lava Dome Eruptions. *Frontiers in Earth Science*, 4:41.
- KOLZENBURG, S., HEAP, M. J., LAVALLÉE, Y., RUSSELL, J. K., MEREDITH, P. G. & DINGWELL, D. B. 2012. Strength and permeability recovery of tuffisite-bearing andesite. *Solid Earth*, 3, 191-198.
- LAMBERT, G., LE CLOAREC, M. F., ARDOUIN, B. & LE ROULLEY, J. C. 1985. Volcanic emission of radionuclides and magma dynamics. *Earth and Planetary Science Letters*, 76, 185-192.
- LOWENSTERN, J. B., BLEICK, H., VAZQUEZ, J. A., CASTRO, J. M. & LARSON, P. B. 2012. Degassing of Cl, F, Li, and Be during extrusion and crystallization of the rhyolite dome at Volcán Chaitén, Chile during 2008 and 2009. *Bulletin of Volcanology*, 74, 2303-2319.
- MACKENZIE, J. M. & CANIL, D. 2008. Volatile heavy metal mobility in silicate liquids: Implications for volcanic degassing and eruption prediction. *Earth and Planetary Science Letters*, 269, 488-496.
- MAGNALL, N., JAMES, M. R., TUFFEN, H. & VYE-BROWN, C. 2017. Emplacing a Cooling-Limited Rhyolite Lava Flow: Similarities with Basaltic Lava Flows. *Frontiers in Earth Science*, 5, 44.

- MAGNALL, N., JAMES, M. R., TUFFEN, H., VYE-BROWN, C., SCHIPPER, C. I., CASTRO, J. M. & DAVIES, A. G. 2018. The origin and evolution of breakouts in a cooling-limited rhyolite lava flow. *GSA Bulletin*.
- MAJOR, J. J. & LARA, L. E. 2013. Overview of Chaitén Volcano, Chile, and its 2008-2009 eruption. *Andean Geology*, 40.
- MATHER, T. A., WITT, M. L. I., PYLE, D. M., QUAYLE, B. M., AIUPPA, A., BAGNATO, E., MARTIN, R. S., SIMS, K. W. W., EDMONDS, M., SUTTON, A. J. & ILYINSKAYA, E. 2012. Halogens and trace metal emissions from the ongoing 2008 summit eruption of Kīlauea volcano, Hawai'i. *Geochimica et Cosmochimica Acta*, 83, 292-323.
- OKUMURA, S., NAKAMURA, M., NAKANO, T., UESUGI, K. & TSUCHIYAMA, A. 2010. Shear deformation experiments on vesicular rhyolite: Implications for brittle fracturing, degassing, and compaction of magmas in volcanic conduits. *Journal of Geophysical Research*, 115, B06201.
- OKUMURA, S. & SASAKI, O. 2014. Permeability reduction of fractured rhyolite in volcanic conduits and its control on eruption cyclicity. *Geology*, 42, 843-846.
- PALLISTER, J. S., DIEFENBACH, A. K., BURTON, W. C., MUÑOZ, J., GRISWOLD, J. P., LARA, L. E., LOWENSTERN, J. B. & VALENZUELA, C. E. 2013a. The Chaitén rhyolite lava dome: Eruption sequence, lava dome volumes, rapid effusion rates and source of the rhyolite magma. *Andean Geology*, 40, 277-294.
- PISTOLESI, M., CIONI, R., BONADONNA, C., ELISSONDO, M., BAUMANN, V., BERTAGNINI, A., CHIARI, L., GONZALES, R., ROSI, M. & FRANCALANCI, L. 2015. Complex dynamics of small-moderate volcanic events: the example of the 2011 rhyolitic Cordon Caulle eruption, Chile. *Bulletin of Volcanology*, 77:3.

- PLAIL, M., EDMONDS, M., HUMPHREYS, M. C. S., BARCLAY, J. & HERD, R. A. 2014. Geochemical evidence for relict degassing pathways preserved in andesite. *Earth and Planetary Science Letters*, 386, 21-33.
- POKROVSKI, G. S., BORISOVA, A. Y. & BYCHKOV, A. Y. 2013. Speciation and Transport of Metals and Metalloids in Geological Vapors. *Reviews in Mineralogy and Geochemistry*.
- REAGAN, M., TEPLEY, F. J., GILL, J. B., WORTEL, M. & HARTMAN, B. 2005. Rapid time scales of basalt to andesite differentiation at Anatahan volcano, Mariana Islands. *Journal of Volcanology and Geothermal Research*, 146, 171-183.
- SAUBIN, E., TUFFEN, H., GURIOLI, L., OWEN, J., CASTRO, J. M., BERLO, K., MCGOWAN, E. M., SCHIPPER, C. I. & WEHBE, K. 2016. Conduit Dynamics in Transitional Rhyolitic Activity Recorded by Tuffisite Vein Textures from the 2008–2009 Chaitén Eruption. *Frontiers in Earth Science*, 4:59.
- SCHIPPER, C. I., CASTRO, J. M., TUFFEN, H., JAMES, M. R. & HOW, P. 2013. Shallow vent architecture during hybrid explosive–effusive activity at Cordón Caulle (Chile, 2011–12): Evidence from direct observations and pyroclast textures. *Journal of Volcanology and Geothermal Research*, 262, 25-37.
- SCHIPPER, C. I., CASTRO, J. M., TUFFEN, H., WADSWORTH, F. B., CHAPPELL, D., PANTOJA, A. E., SIMPSON, M. P., Le Ru, E. C. (2015). Cristobalite in the 2011–2012 Cordón Caulle eruption (Chile). *Bulletin of Volcanology*, 77:34(5). <https://doi.org/10.1007/s00445-015-0925-z>
- SILVA PAREJAS, C. L., L. E.; BERTIN, D.; AMIGO, A.; OROZCO, G. 2012. The 2011–2012 eruption of Cordón Caulle volcano (Southern Andes): Evolution, crisis management and current hazards. *EGU General Assembly 2012*. Vienna, Austria.



- STASIUK, M. V., BARCLAY, J., CARROLL, M. R., JAUPART, C., RATTE, J. C., SPARKS, R. S. J. & TAIT, S. R. 1996. Degassing during magma ascent in the Mule Creek vent (USA). *Bulletin of volcanology*, 58, 117.
- SYMONDS, R. B., ROSE JR, W. I., REED, M. H., LICHTER, F. E. & FINNEGAN, D. L. 1987. Volatilization, transport and sublimation of metallic and non-metallic elements in high temperature gases at Merapi Volcano, Indonesia. *Geochimica et Cosmochimica Acta*, 51, 2083-2101.
- THOMAS, J. B., BODNAR, R. J. , SHIMIZU, N., CHESNER, C. A.; 2003. Melt Inclusions in Zircon. *Reviews in Mineralogy and Geochemistry*, 53, 63-87.
- TUFFEN, H. & DINGWELL, D. 2005. Fault textures in volcanic conduits: evidence for seismic trigger mechanisms during silicic eruptions. *Bulletin of Volcanology*, 67, 370-387.
- TUFFEN, H., DINGWELL, D. B. & PINKERTON, H. 2003. Repeated fracture and healing of silicic magma generate flow banding and earthquakes? *Geology*, 31, 1089-1092.
- TUFFEN, H., JAMES, M. R., CASTRO, J. M. & SCHIPPER, C. I. 2013. Exceptional mobility of an advancing rhyolitic obsidian flow at Cordon Caulle volcano in Chile. *Nat Commun*, 4, 2709.
- TURNER, S., BLACK, S. & BERLO, K. 2004.  $^{210}\text{Pb}$ – $^{226}\text{Ra}$  and  $^{228}\text{Ra}$ – $^{232}\text{Th}$  systematics in young arc lavas: implications for magma degassing and ascent rates. *Earth and Planetary Science Letters*, 227, 1-16.
- VAN HINSBERG, V. J., BERLO, K., MIGDISOV, A. A. & WILLIAMS-JONES, A. E. 2016.  $\text{CO}_2$ -fluxing collapses metal mobility in magmatic vapour. *Geochemical Perspectives Letters*, 169-177.

- WAHRENBERGER, C. 2002. Volatile trace-element transport in high-temperature gases from Kudriavy volcano (Itrup, Kurile Islands, Russia). *The Water-Rock Interactions, Ore Deposits, and Environmental Geochemistry: A tribute to David A. Crerar*.
- WEBSTER, J. D. 1990. Partitioning of F between H<sub>2</sub>O and CO<sub>2</sub> fluids and topaz rhyolite melt. *Contributions to Mineralogy and Petrology*, 104, 424-438.
- WHITE, W. M. 2013. *Geochemistry*, John Wiley & Sons.
- WILLIAMS-JONES, A. E. & HEINRICH, C. A. 2005. 100th Anniversary Special Paper: Vapor Transport of Metals and the Formation of Magmatic-Hydrothermal Ore Deposits. *Economic Geology*, 100, 1287-1312.
- WILLIAMS-JONES, A. E., MIGDISOV, A. A., ARCHIBALD, S. M. & XIAO, Z. 2002. *Vapor-transport of ore metals*. *The Water-Rock Interactions, Ore Deposits, and Environmental Geochemistry: A tribute to David A. Crerar*.
- ZAJACZ, Z., HALTER, W. E., PETTKE, T. & GUILLONG, M. 2008. Determination of fluid/melt partition coefficients by LA-ICPMS analysis of co-existing fluid and silicate melt inclusions: Controls on element partitioning. *Geochimica et Cosmochimica Acta*, 72, 2169-2197.
- ZELENSKI, M. E., FISCHER, T. P., DE MOOR, J. M., MARTY, B., ZIMMERMANN, L., AYALEW, D., NEKRASOV, A. N. & KARANDASHEV, V. K. 2013. Trace elements in the gas emissions from the Erta Ale volcano, Afar, Ethiopia. *Chemical Geology*, 357, 95-116.

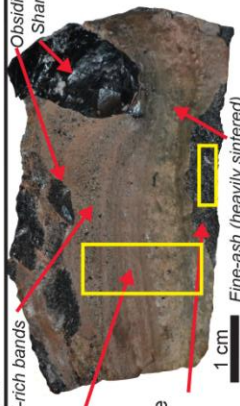
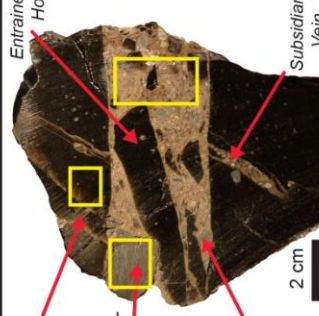
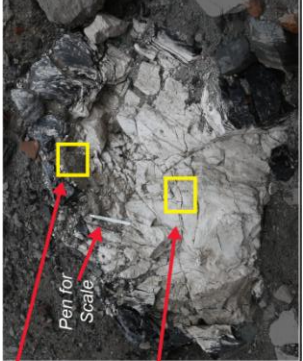
## 8. Table and Figure Captions

(Full Page) Figure 1: Summary of key textural features of samples from Cordon Caulle (Flow 1 & Bombs 1-5) and Chaitén (Bombs A & B). Sub-samples are noted in bold and briefly described. Additional descriptions in italics. Yellow boxes are representative of material analysed for each sub-sample.

Figure 1:

Size	Sub-Sample Descriptions	Sub-Sample Interpretations
<b>Flow 1</b> ~10 cm sub-sample of northern breakout lobe	Breakout lobe at flow front. Breakouts are described by Schipper et al. (2015) and Magnall et al. (2018) as vesiculated obsidian with ~40 % plagioclase and 10 % pyroxene microlites set in a glass groundmass. No tuffsite veins are present in the flow samples. Vesicles in this sample are <1 cm in size, are elongate to spherical, and coated with vapour-deposited cristobalite. <b>Beige:</b> Rounded to elongate cm-sized clasts. Vesicle size increases towards clast centre. <b>Black:</b> Rarer clasts, both vesiculated and dense clasts present. <i>Interstitial matrix material is dark-grey to black in colour and forms sintered veins between larger clasts. Fine-grained glass can be oxidised to orange-red in certain samples (similar to this).</i>	Parallel cristobalite bands are thought to record vesicle collapse.
<b>Bomb 1</b> ~10 cm sub-sample of a ~30 cm scale bread-crust bomb	<b>Exterior:</b> A metre-scale grey pumice bomb. Quenched, light grey, vesiculated (mm-sized) pumice. Melt rinds at the vein-host interface. <b>Vein:</b> Located near bomb rim, 1-3 cm wide. Pale pink colour (oxidation), with fine and coarse-grained laminations and some inflated clasts. Subsidiary and injections veins present offshooting from main vein. <b>Interior:</b> Vesicles (10s cm) due to bomb expansion post-ejection. Smaller vesicles <1 cm from vein walls result of local syn-eruptive or post-eruptive degassing into vein. Volatile depleted melt foamed less than bomb interior far from vein.	No tuffsite vein present but breccia bombs resemble tuffsite vein fill material. It is likely breccias represent the same process fracturing and gas fluxing process in the upper conduit as tuffsites.
<b>Bomb 2</b> Sub-sample of a ~1.5 m scale bread-crust bomb	<b>Host:</b> Highly sheared, vesiculated tube pumice. Sheared vesicles run in parallel orientation to vein. Tuffsite material found in host vesicles. <b>Outer Vein:</b> Pale pink (oxidation), fine-grained sintered ash in concave laminations. Tuffsite material is variably sintered. <b>Inner Vein:</b> Sintered ash, colour grades from orange to white.	Melt rinds at vein-host interface could be due to shearing or material quenching upon ejection. Tuffsite textures indicative of fluidised flow. Inflated clasts within beds of coarse-grained fill indicate material of different volatile contents were tapped when fracture was open and have subsequently inflated differently as bomb was ejected. Vein shape altered by melt relaxation and bomb inflation.
<b>Bomb 3</b> ~15 cm long pumice bomb with large ash-filled vesicles	<b>Host:</b> Highly sheared, vesiculated tube pumice. Sheared vesicles run in parallel orientation to vein. Tuffsite material found in host vesicles. <b>Outer Vein:</b> Pale pink (oxidation), fine-grained sintered ash in concave laminations. Tuffsite material is variably sintered. <b>Inner Vein:</b> Sintered ash, colour grades from orange to white.	Tuffsite infiltrating into host implies host vesicularity developed and connected prior to tuffsite formation. Changing vein colour suggests it started open to the atmosphere (and was heavily oxidised) becoming less open (and oxidised) with time.

Cordon Caulle

Size	Sub-Sample Descriptions	Sub-Sample Interpretations
Bomb 4 ~15 cm bomb fragment	<p><b>Vein:</b> Multiple pink-orange laminations distinguished by variable particle sintering, particle-size, % obsidian ash and vesicularity. Banding deflected around large, dense-obsidian shards.</p> <p><b>Host:</b> Black vesiculated obsidian. Melt relaxation at the host-vein interface (not shown). Vesicles (mm-sized) and rare mm-sized plagioclase crystals are observed.</p> 	<p>Observations from this and other tuffisite veins at Cordón Caulle suggest later veins have more variability in vein components.</p>
Bomb 5 ~8 cm wide small vesicular bomb	<p>Black vesicular bomb fragment with no vein. The bomb rim is quenched and vesicles are mm scale. There are rare plagioclase crystals visible (1-2 mm in size). Material adhered to the outside of the samples is oxidised ash and mm-sized obsidian shards (surface material was not analysed). The cone structure around the vein is predominantly composed of pumice bombs, grey and black in colour, varying from cm scale to metre scale.</p>	<p>Ash and obsidian shards were likely welded to the bomb surface when they were still hot.</p>
Bomb A Sub-sample from a ~0.5 m wide dense obsidian bomb	<p><b>Host:</b> Dense obsidian, hosting a 3 cm-wide tuffisite vein and subsidiary veins. Host, vein and clasts are described in detail by Saubin et al. (2016).</p> <p><b>Banded Clast:</b> cm-sized, sub-rounded clast with uneven boundaries. Have greatest size range of vein clasts (mm to cm sized) and most irregular shapes. Are heterogeneous with glassy and SiO<sub>2</sub>-enriched bands (~93 wt. %). Latter bands correspond to fractured areas, have greater porosity and crystallinity.</p> <p><b>Vein:</b> ~3 cm wide, parallel-walled vein composed of banded (~35 %), dense (~42 %) and vesicular (~22 %) clasts in a fine-grained, oxidised matrix.</p> 	<p>SiO<sub>2</sub>-enriched bands interpreted as zones of cristobalite precipitation. Banded Clast interpreted as non-juvenile material from previous activity in caldera.</p> <p><b>Vein Matrix &amp; Clasts</b> represents bulk vein.</p>
Bomb B Two ~30 cm sub-samples from a ~1.5 m bomb with dense rind and pumiceous core	<p><b>Exterior:</b> 2-8 cm dense, glassy rind, cracks &lt;10 cm into interior. Grades into pumice interior. Thin black bands of glass are found in the transition zone between the bomb and interior. Open (&lt;10 cm deep) cooling fractures in rind.</p> <p><b>Interior:</b> Elongate clasts of white pumice surrounded by mm-wide grey bands of dense glass. There is visible micro-porosity in the interior of clasts. Secondary bread-crusting (&lt;1 cm) can be found on the surface of some of the white pumice clasts. Sample comes from an area with more abundant grey bands in the bomb interior. Interior also has &lt;10 cm long open fractures.</p> 	

Cordón Caulle

Chalten

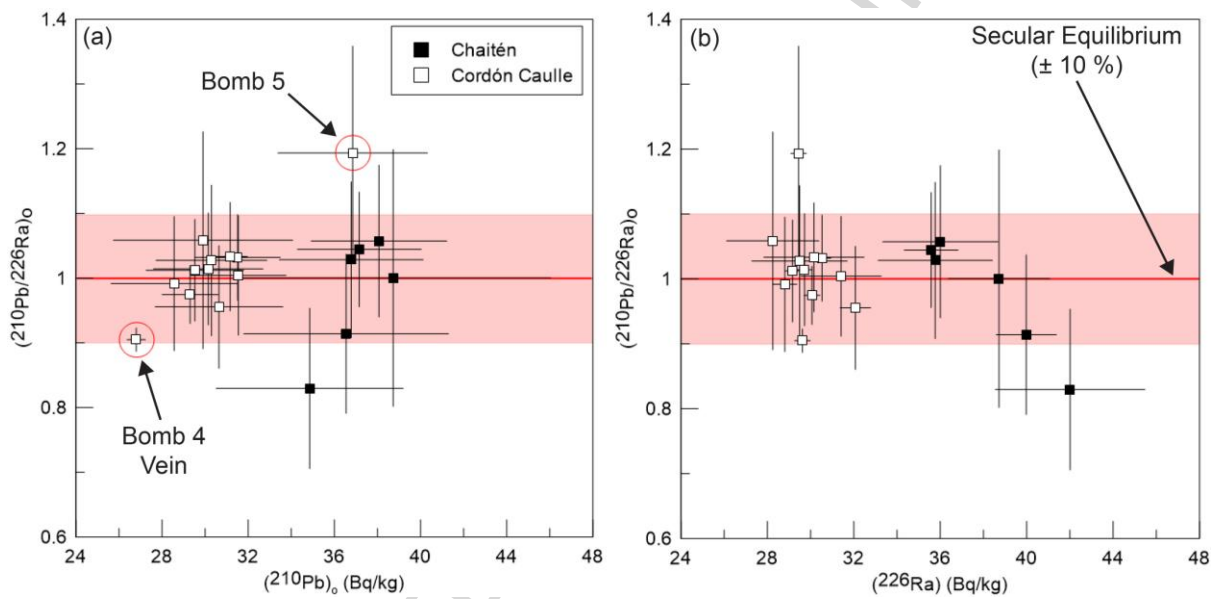
Table 1: Activities and activity ratios (back calculated to time of eruptions) of samples and sub-samples analysed via alpha spectrometry ( $^{210}\text{Pb}$ ) and TIMS ( $^{226}\text{Ra}$ ).

Table 1:

Sample ID	$(^{210}\text{Pb})_o$ (Bq/kg)	$\pm 2 \text{ SD}$ (Bq/kg)	$(^{226}\text{Ra})$ (Bq/kg)	$\pm 2 \text{ SD}$ (Bq/kg)	$(^{210}\text{Pb}/^{226}\text{Ra})_o$	$\pm 2 \text{ SD}$
Bomb A Host	37.16	2.88	35.58	1.25	1.04	0.09
Bomb A Vein Matrix & Clasts	38.07	3.15	36.01	2.67	1.06	0.12
Bomb A Vein Matrix	38.73	7.32	38.72	2.35	1.00	0.20
Bomb A Banded Clast	36.55	4.76	39.98	1.40	0.91	0.12
Bomb B Interior	36.79	3.34	35.77	2.65	1.03	0.12
Bomb B Exterior	34.85	4.34	42.01	3.46	0.83	0.12
Flow 1	29.91	4.16	28.25	2.14	1.06	0.17
Bomb 1 Black	30.30	2.58	29.49	2.21	1.03	0.12
Bomb 1 Beige	29.52	2.27	29.17	0.35	1.01	0.08
Bomb 2 Exterior	31.51	1.98	30.53	0.41	1.03	0.07
Bomb 2 Vein	30.65	2.97	32.07	0.71	0.96	0.09
Bomb 2 Interior	29.31	1.30	30.07	0.37	0.97	0.04
Bomb 3 Host	31.16	0.81	30.16	2.32	1.03	0.08
Bomb 3 Outer Vein	31.54	2.22	31.41	1.86	1.00	0.09
Bomb 3 Inner Vein	30.15	2.55	29.72	0.36	1.01	0.09
Bomb 4 Host	28.57	2.94	28.81	0.56	0.99	0.10
Bomb 4 Vein	26.81	0.43	29.62	0.36	0.90	0.02
Bomb 5	36.85	3.47	29.45	0.36	1.19	0.17
BCR-2*	21.62	1.49	21.74	3.22		

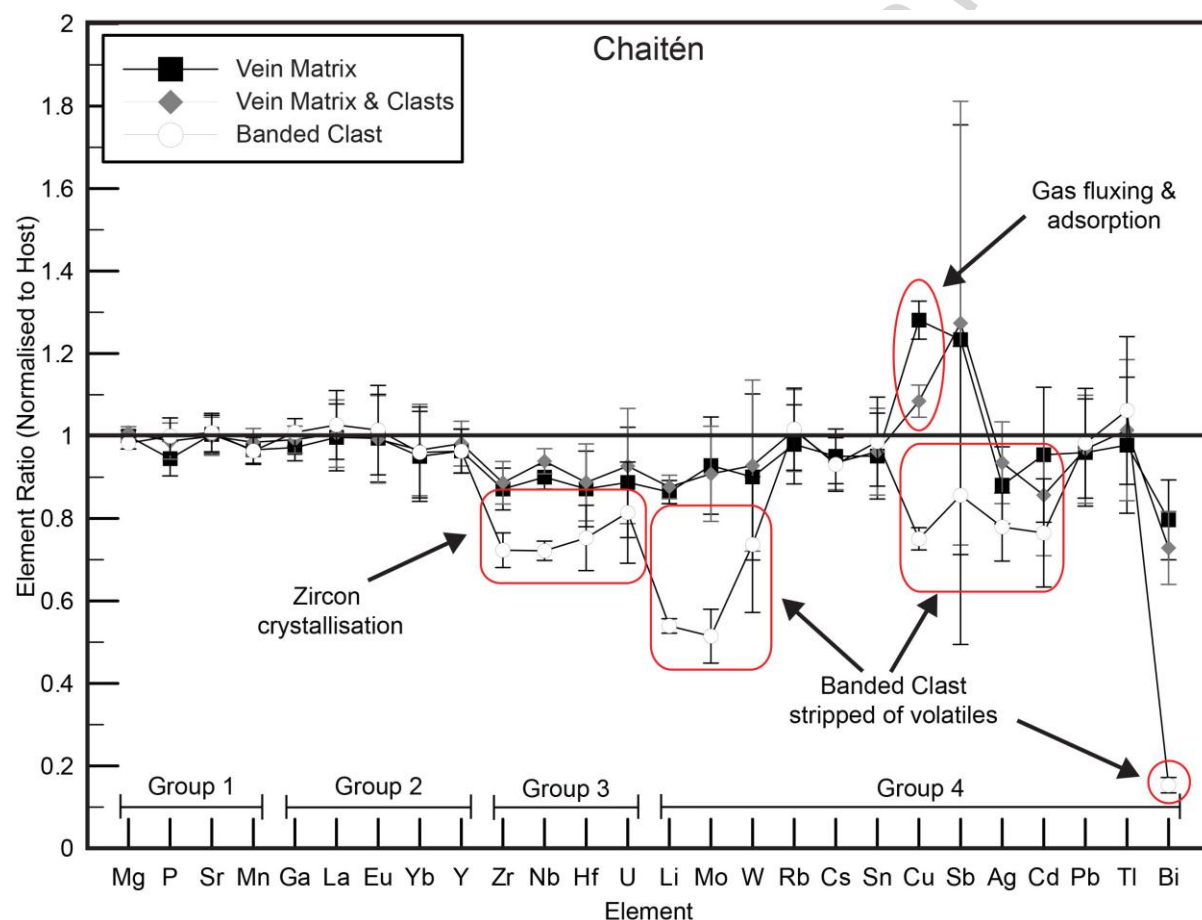
\*Average values for BCR-2, 5 duplicates were run for  $^{210}\text{Pb}$  and 3 duplicates were run for  $^{226}\text{Ra}$ .

(2-column) Figure 2:  $(^{210}\text{Pb}/^{226}\text{Ra})_o$  versus (a)  $(^{210}\text{Pb})_o$  and (b)  $(^{226}\text{Ra})$  showing the excesses and deficits in the Cordon Caulle samples (white) are solely due to  $^{210}\text{Pb}$  variation. Chaitén samples (black) show  $^{226}\text{Ra}$  variability. Annotations are outliers discussed in Section 4.4. The red box denotes a 10 % error window, equivalent to the average two standard deviation value on calculated ratios in Table 1.



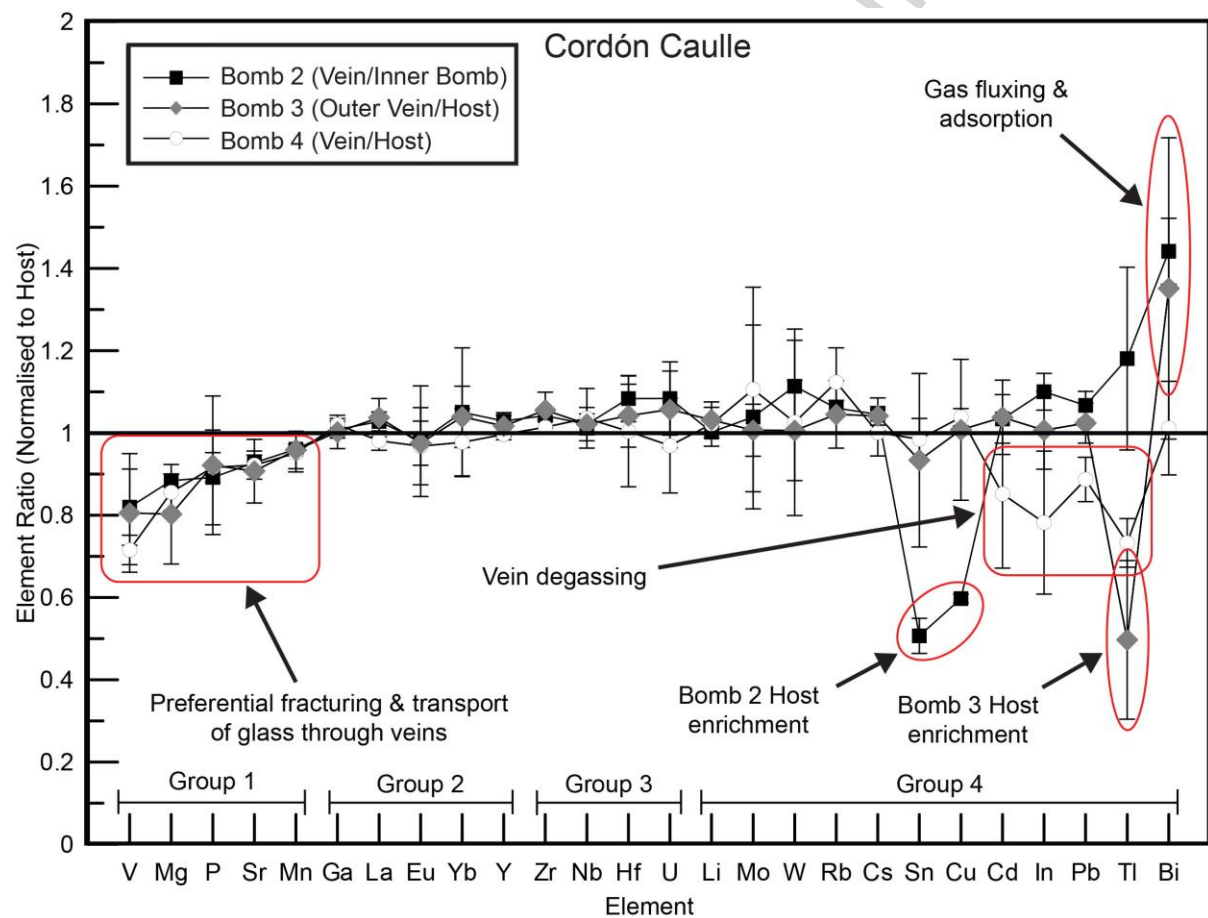


(2-column) Figure 3: Select elemental concentrations of Vein Matrix, Vein Matrix & Clasts (bulk tuffisite) and Banded Clast normalised to Bomb A Host composition (Chaitén Volcano). Depletions in HFSEs and volatile elements (e.g. Mo, Li, Bi) are evident in both clast and vein samples, as is Cu enrichment in the vein. Errors are 2 standard deviation.

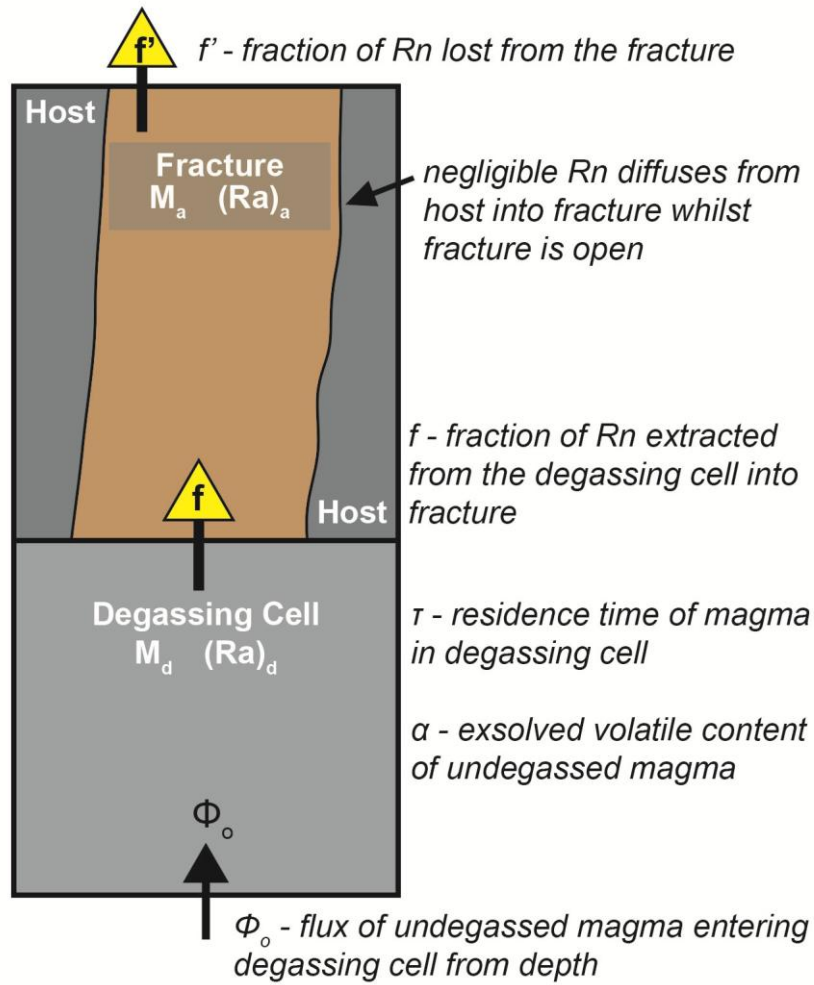




(2-column) Figure 4: Element concentrations from select tuffisite veins from Cordon Caulle normalised to host composition. Bomb 2 (vein) is normalised to Bomb 2 (Interior) concentration (black squares). Bomb 3 (Outer Vein) is normalised to Bomb 3 (Host) (grey diamonds) and the Bomb 4 (vein) is normalised to Bomb 4 (Host) (white circles). Errors are 2 standard deviation.



(Single Column) Figure 5: Schematic model of a fracture sourcing Rn from a degassing cell. Yellow arrows indicate gas transfer in and out of the fracture. Magma fluxes ( $\Phi_o$ ) into a degassing cell that has a mass,  $M_d$ , and Ra activity,  $(Ra)_d$ , and volatiles exsolve. Volatiles, including Rn, are extracted from the degassing cell and into the fracture (mass,  $M_a$ , and Ra activity,  $(Ra)_a$ ),  $f$  denotes the fraction of Rn extracted from the degassing cell. Volatiles outgas through the fracture to the surface,  $f'$  denotes the fraction of Rn lost from the fracture. This model assumes all Rn that enters the fracture comes solely from the degassing cell and not the tuffsite host thus calculated mass ratios (R values) can be used to estimate the upper limit of the volume size of the degassing cell.



(Single Column) Figure 6: Contoured plot showing required  $R$  values to generate certain  $(^{210}\text{Pb}/^{226}\text{Ra})$  for a known fracture lifespan assuming  $\tau = 0.019$ ,  $f = 1$  and  $f^* = 0.5$ . Black lines highlight the required  $R$  values, given minimum (1.6 hour) and maximum (7.5 hour) lifespan estimates of example fractures from Chaitén, to generate a  $(^{210}\text{Pb}/^{226}\text{Ra}) = 1.10$  (see Section 4.2) (Castro et al., 2012).

